BRNO UNIVERSITY OF TECHNOLOGY

Faculty of Electrical Engineering
and Communication

BACHELOR'S THESIS

Brno, 2024 Hana Daová

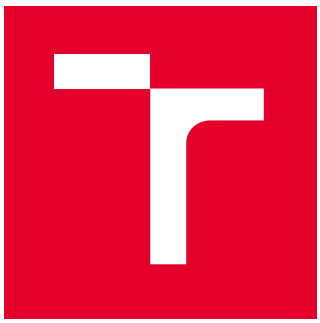

BRNO UNIVERSITY OF TECHNOLOGY

VYSOKÉ UČENÍ TECHNICKÉ V BRNĚ

FACULTY OF ELECTRICAL ENGINEERING AND COMMUNICATION

FAKULTA ELEKTROTECHNIKY
A KOMUNIKAČNÍCH TECHNOLOGIÍ

DEPARTMENT OF RADIO ELECTRONICS

ÚSTAV RADIOELEKTRONIKY

BLE RANGING KEY FOB ANTENNA

ANTÉNA DO KLÍČKU AUTA PRO BLE RANGING

BACHELOR'S THESIS
BAKALÁŘSKÁ PRÁCE

AUTHOR — **Hana Daová**
AUTOR PRÁCE

SUPERVISOR — **prof. Dr. Ing. Zbyněk Raida**
VEDOUCÍ PRÁCE

BRNO 2024

BRNO UNIVERSITY OF TECHNOLOGY
FACULTY OF ELECTRICAL ENGINEERING AND COMMUNICATION

Bachelor's Thesis

Bachelor's study program **Electronics and Communication Technologies**

Department of Radio Electronics

Student: Hana Daová ***ID:*** 230238

Year of study: 3 ***Academic year:*** 2023/24

TITLE OF THESIS:

BLE ranging key fob antenna

INSTRUCTION:

Within the project, an antenna to be integrated into a key fob is designed and implemented. The antenna is connected to a module for wireless measurements of a distance between a car and a key fob. The ranging uses Bluetooth Low Energy (BLE) Channel Sounding (CS).

An overview of suitable antennas is prepared. For promising antennas, numerical models are developed in ANSYS HFFS. Comparing models, the most suitable one is selected. The selected antenna is optimized for NXP KW45 board. The optimized antenna is manufactured and its functionality is verified by a set of ranging experiments performed both in a chamber and a real environment.

RECOMMENDED LITERATURE:

[1] BALANIS, C.A. Antenna Theory: Analysis and Design, 4th Edition. Hoboken (New Jersey): John Wiley & Sons, 2016. ISBN: 978-1-118-64206-1.

[2] -, Channel Sounding | Bluetooth® Technology Website [online]. Copyright © 2023 Bluetooth SIG. [cit. 23.05.2023]. Available: https://www.bluetooth.com/specifications/specs/channel-sounding/

Date of project specification: 16.2.2024 ***Deadline for submission:*** 27.5.2024

Supervisor: prof. Dr. Ing. Zbyněk Raida

doc. Ing. Lucie Hudcová, Ph.D.
Chair of study program board

Abstract

This bachelor's thesis consists of designing an antenna that would fit into a car key fob and would be able to measure distance between a car and its key via a microcontroller unit by channel sounding method. The antenna is designed for bandwidth 2.4 GHz in which the Bluetooth Low Energy standard operates. In this project, the issue of selecting the most suitable antenna for these purposes is analysed by comparing numerical models created and simulated in ANSYS HFSS. Based on the acquired data, the most suitable antenna is afterwards optimized for the usage with NXP KW45 board and its optimized version is manufactured to verify its functionality.

Keywords

Planar antenna, coplanar waveguide, Bluetooth Low Energy, BLE, channel sounding, distance measurement, ANSYS HFSS

Abstrakt

Tato bakalářská práce sestává z návrhu antény do klíčku auta, jež bude schopna pomocí mikrokontroléru metodou channel sounding měřit vzdálenost mezi autem a jeho klíčkem. Anténa je navržena pro pásmo 2,4 GHz, ve kterém pracuje technologie Bluetooth Low Energy. V projektu je porovnáním několika numerických modelů, vytvořených a simulovaných v programu ANSYS HFSS, rozebrána problematika výběru vhodného typu antény. Na základě získaných poznatků je následně nejvhodnější anténa optimalizována pro použití s čipem NXP KW45 a její optimalizovaná verze je pak realizována za účelem experimentálního ověření funkčnosti.

Klíčová slova

Planární anténa, koplanární vlnovod, Bluetooth Low Energy, BLE, channel sounding, měření vzdálenosti, ANSYS HFSS

Rozšířený abstrakt

Bluetooth Low Energy (BLE), spadající pod klasický Bluetooth od verze 4.0, je technologie pracující v pásmu 2,4 GHz, která je určená k bezdrátové komunikaci mezi dvěma a více zařízeními. V dnešní době má již celkem rozsáhlé využití v různých odvětvích jako jsou například zdravotnictví, bezpečnostní systémy, sport či automobilový průmysl. Její největší předností je bezpochyby její nízká spotřeba energie. Zařízení používající tuto technologii mohou vydržet až roky bez nabíjení, a to díky tomu, že se udržují většinu času v režimu spánku a aktivně sdílí data jen pokud jsou k tomu vyzvána. Další výhodou této technologie je její kompatibilita s klasickým Bluetooth standardem, který je velmi hojně využívaný ve většině operačních systémů a tím pádem má velký potenciál v budoucnu rozšířit své využití i do dalších oblastí.

Pod BLE spadá funkce channel sounding, která při komunikaci mezi zařízeními shromažďuje informace, z nichž se dá vyhodnotit jejich vzájemná poloha a vzdálenost. Jedná se o funkci, která výrazně napomohla ke zvýšení přesnosti ve vyhodnocování vzdálenosti mezi těmito zařízeními a která nebyla součástí předchozích verzí Bluetooth. Není tedy v současném světě tak dlouho a stále se vyvíjí, což nabízí prostor k jejímu dalšímu zkoumání.

Za účelem umožnění rychlejšího pokroku v již zmiňovaných odvětvích (především automobilového průmyslu), vyvinula společnost NXP Semiconductors programovatelnou elektronickou desku, která má v sobě zabudované jádro s BLE. Celý výrobek je řízen mikrokontrolérem NXP KW45 a dají se k němu připojit různé periferie přes různé konektory jako je například CAN, LIN či SMA. Tato komponenta v tomto projektu poslouží jako zprostředkovatel technologie BLE.

Cílem této práce je návrh a optimalizace antény, která by se dala v pásmu 2,4 GHz pomocí čipu NXP KW45 použít jako měřič vzdálenosti mezi autem a jeho klíčkem. Stávající technologie fungující na obdobném principu pracuje na frekvenci 433,92 MHz a nazývá se remote keyless entry. Ona technologie na základě vzdálenosti umožňuje uživateli otevřít auto, bez nutnosti vyndat klíček z kapsy. Jelikož by zmiňovaná anténa měla být implementovatelná do klíčku auta, je při návrhu kladen důraz především na její velikost.

Na začátku je navrženo několik různých modelů antén, které jsou mezi sebou následně porovnány z hlediska velikosti, směrových charakteristik a impedančního přizpůsobení. Dále je nejvhodnější anténa optimalizována pro použití s čipem a je otestována její funkčnost jak ve stíněné komoře, tak v reálném prostředí. Vzhledem k tomu, že by anténa měla sloužit jako prvek zabudovaný v klíčku, je také prozkoumán vliv přítomnosti lidské tkáně v jejím blízkém okolí.

Bibliographic citation

DAOVÁ, Hana. *Anténa do klíčku auta pro BLE ranging.* Brno: Brno University of Technology, Faculty of electrical engineering and communications, Dept. of telecommunications, 2024. 50 p. Bachelor's thesis. Advised by prof. Dr. Ing. Zbyněk Raida.

Author’s Declaration

Author:	*Hana Daová*
Author’s ID:	*230238*
Paper type:	*Bachelor’s Thesis*
Academic year:	*2023/24*
Topic:	*BLE ranging key fob antenna*

I declare that I have written this paper independently, under the guidance of the advisor and using exclusively the technical references and other sources of information cited in the project and listed in the comprehensive bibliography at the end of the project.

As the author, I furthermore declare that, with respect to the creation of this paper, I have not infringed any copyright or violated anyone’s personal and/or ownership rights. In this context, I am fully aware of the consequences of breaking Regulation S 11 of the Copyright Act No. 121/2000 Coll. of the Czech Republic, as amended, and of any breach of rights related to intellectual property or introduced within amendments to relevant Acts such as the Intellectual Property Act or the Criminal Code, Act No. 40/2009 Coll., Section 2, Head VI, Part 4.

.

Brno, May 27, 2024 ----------

author’s signature

Acknowledgement

The completion of this bachelor's thesis would not have been possible without my advisor's, prof. Dr. Ing. Zbyněk Raida's, professional support, patience and great guidance throughout project solving and therefore I would like to thank him very much for all of that. His invaluable words of advice kept me going. I am also grateful to doc. Ing. Jaroslav Láčík, Ph.D. for his time and help with antenna manufacturing. Thanks should also go to Ing. Tomáš Mikulášek, Ph.D., Ing. Vojtěch Bednarský and Ing. David Kuřátko for their practical suggestions.

Brno, May 27, 2024 ----------

Author's signature

Contents

.

FIGURES

TABLES

INTRODUCTION

The main goal of this bachelor's thesis is designing an antenna suitable for wireless measurements of distance between a car and its key fob via channel sounding method that falls under Bluetooth Low Energy (BLE) technology which operates in the 2.4 GHz band. The biggest advantage of BLE is its low power consumption allowing devices using this technology to work up to several years without charging.

Since the antenna is meant to be implemented into a car key fob, the design process is primarily focused on the antenna size. For this reason, it is crucial to consider planar antennas which are formed by a very thin layer of an electrical conductor deposited on a dielectric substrate.

The first chapter is dedicated to a brief description of Bluetooth Low Energy technology and its connection to the channel sounding method. Furthermore, a closer look is also taken at the antenna design process itself. For realising the numerical models, a simulation software ANSYS HFSS was used. The antennas are then each compared among themselves considering their size, impedance matching, radiation pattern and gain. Optimization of the most suitable antenna for this application is described in chapter 4. Finally, the comparison between the simulated and the manufactured antenna is provided and can be found in chapter 5.

1. THEORETICAL BACKGROUND

The following text briefly introduces the theory that was considered when creating antenna models for this bachelor's work. It should provide more awareness of Bluetooth Low Energy technology and channel sounding or it can just refresh the reader's knowledge about this topic.

1.1 Bluetooth Low Energy

In 2010, the Bluetooth Low Energy technology (BLE) was publicly presented for the first time as a part of Bluetooth 4.0. This standard allows a short range simple wireless communication between two devices or among more than two devices. Nowadays, it coexists with its predecessor, the classical Bluetooth, from which it is derived. Both technologies are widely used in various areas such as sports, security systems, health care, automotive industry, music industry and many more.

As it can already be presumed from the BLE title itself, the technology's fundamental advantage lies in its low power consumption. This quality is used by devices with a small dataflow, so the battery life, considering today's available technical options, is maximized. For example, various sensors using a coin battery and communicating with smartphones, tablets or computers would be such devices. The low power consumption is maintained by keeping the connected units in sleep mode most of the time and enabling their active communication only on command.

From a technical perspective, this standard is based on short packets transmission on short range (up to 50 m) using a combination of frequency division multiple access (FDMA), time division multiple access (TDMA) and frequency hopping spread spectrum (FHSS). BLE technology operates in the license-free ISM radio band 2.4 GHz, which is defined as an interval of frequencies from 2400 MHz to 2483.5 MHz. The packets are always transmitted in only one of the forty radiofrequency (RF) communication channels and that is how FDMA is applied. The mentioned channels' centre frequencies are parted from one another by 2 MHz range each in a frequency band from 2402 MHz to 2480 MHz. By setting up a fixed transmission time for the transmitter and a fixed time delay after which the receiver reacts to the transmitter, the application of TDMA is secured. To rapidly decrease the possibility of the signal interference, a form of FHSS called adaptive frequency hopping (AFH) is used while transmitting packets. As mentioned before, the data are sent via only one RF channel but adding AFH, the RF channel used is being changed at time. Every channel that is evaluated as busy and noisy is avoided. [5]

1.1.1 Bluetooth Low Energy vs. classical Bluetooth technology

Regardless of the two technologies name similarity, Bluetooth and BLE, there are certain

reasons behind their coexistence and therefore differences can be found between them. Meanwhile classical Bluetooth is commonly used among devices continually transmitting higher data rates (such as wireless headphones), BLE can rather be found in devices that transmit less data and less often. Nowadays it is mainly wearable medical devices which scan user's vital functions such as blood pressure, heart rate or blood sugar level. Besides those, physical activity sensors implemented into smart watches are also worth mentioning. These applications of BLE emphasise the need for a long battery life which is associated with long-term low power consumption. [21]

Although classical Bluetooth technology has more RF communication channels available (79 channels), has higher data rate and is ranged up to 100 m, compared to BLE, it also has higher energy consumption which is unwanted in our application. Therefore, BLE is more suitable for these purposes which consist of a car key fob that would be inactive most of the time, activated on command.

1.1.2 Utilization

Most of the cars today have their security key which can be used not only mechanically but also wirelessly via so-called remote keyless entry (RKE) system. This system provides a possibility to unlock user's car by only being nearby the vehicle and some of the car models allow even remote starting. [1], [22]

A small transmitter implemented in a key fob and a receiver built in a car are used within RKE. In Japan and the United States, both antennas are set to frequency 315 MHz. In Europe, their frequency is set to 433.92 MHz. By using BLE technology via a microcontroller unit KW45 from NXP Semiconductors company, new application possibilities at new frequency band can be reached in the future. Since BLE is compatible with classical Bluetooth and both technologies are commonly used in most of the operation systems, the options could be very various. [1]

1.2 Channel Sounding

Being a part of BLE, Channel Sounding (CS) significantly increases the precision of distance and position evaluation for Bluetooth. This function closely analyses the environment in which the wirelessly communicating devices are present. During the CS procedure, data which can be further mathematically processed, and which help with the distance evaluation are created.

CS has 4 types of steps. The first mode (mode-0) calibrates one communicating device to the other in terms of frequency and timing. In the next mode (mode-1), round-trip time (RTT) packets are being exchanged between the devices. The third mode (mode-2) consists of tones transmission which determines phase and amplitude of the RF communication channel. Finally, the last mode (mode-3) is combination of mode-1 or mode-2 repetition as needed. [6]

From the BLE perspective, there is no specific algorithm for CS distance evaluation. However, two simplified mathematical models can be used to describe the procedure. One of them uses RTT packets provided in mode-1 and mode-3. The other one is based on utilization of the information about phase and amplitude of the transmitted data provided in mode-2 and mode-3.

1.2.1 Distance estimate using RTT packets

For distance evaluation using RTT packets, time of departure (ToD) and time of arrival (ToA) are considered. Both are used for time of flight (ToF) calculation. [6]

The distance between two devices x can then be evaluated as

$$x = \frac{(ToA_i - ToD_i) - (ToD_r - ToA_r)}{2} \cdot c \,, \tag{1.1}$$

where ToA_i is time of data arrival towards the initiator, ToD_i is time of data departure from the initiator, ToD_r is time of data departure from the reflector, ToA_r is time of data arrival towards the reflector and c is the speed of light in vacuum. This method is rather used for larger distances estimation. For better visualisation. see the figure below:

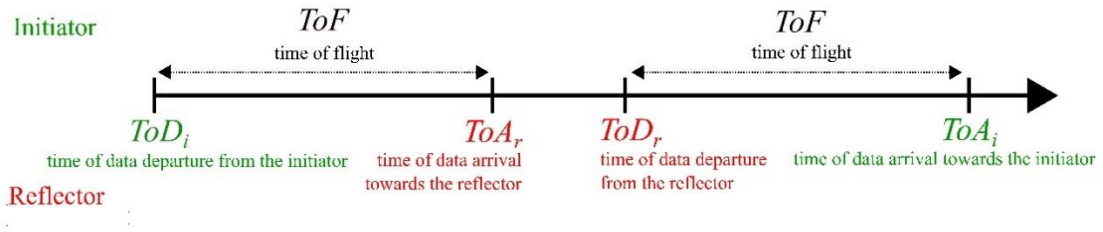

Fig. 1.1 Distance estimate using RTT packets

1.2.2 Distance estimate using amplitude and phase of the data

More precise distance and position estimation for shorter distances is achieved by using phase-based ranging (PRB). A tone is transmitted.

Generally, a sinusoidal signal (a tone) is shifted by its one wavelength when the phase shift is 2π. May c be the speed of light in vacuum and f the tone frequency. Wavelength λ can then be calculated as

$$\lambda = \frac{c}{f} \,. \tag{1.2}$$

Consider a transmission of two tones, one with frequency f_1 and the other one with frequency f_2. The information about phase shift can be used for distance evaluation

$$x = \frac{c \cdot \Delta\varphi}{2\pi \cdot |f_1 - f_2|} \,, \tag{1.3}$$

where c is the speed of light in vacuum and $\Delta\varphi$ is data phase shift between two devices.

1.3 NXP KW45

NXP KW45 microcontroller unit (MCU) is a wireless electronic component that works within BLE band. It has a high potential of enhancing the development in automotive industry and other industrial branches. The main goal of its applications are for example secure car access, keyless entry or Passive Entry/Passive Start (PEPS). It also supports positioning and localization thanks to the integrated BLE radio core and thus, its usage within this project is reasonable. [13]

As the chip is available in many forms, it can be bought alone for user's own implementation or already implemented on ready-to-use electronic boards. In our application, the KW45B41Z EVK is considered.

1.3.1 Microcontroller evaluation kit

Fig. 1.2 NXP KW45B41Z EVK, taken from [13]

The EVK in the board's name stands for evaluation kit. The kit supports CAN, LIN and Arduino connection, and it also has a mikroBUS socket. In case no antenna is connected to the board, a PCB planar inverted F antenna, which can be seen in the figure 1.2, can be used as a wireless transmitter or receiver in applications. This antenna can be bypassed and replaced by another testing antenna using the mounted SMA RF (F) connector. [13]

2. ANTENNAS DESIGN AND SIMULATION

Creating an antenna that meets specific criteria involves designing and simulating its numerical model in a suitable software. For this application, Ansys Electronic Desktop program, specifically the part called ANSYS HFFS, was used. In addition, for simplifying the designing process, available calculator freeware for evaluating the waveguide characteristics was used. Finally, MATLAB was used for plotting antenna characteristics.

A primary layout of the suitable antennas may be found within this chapter. The antenna shapes are chosen considering the size of a car key fob, and their radiation patterns are presented.

2.1 ANSYS HFSS

Ansys HFSS (High Frequency Structure Simulator) is a commercial software based on 3D electromagnetic field simulation. Its purpose is found in designing and simulating various electronic components such as printed circuit boards, connectors, filters or antennas. 47[2]

The program uses finite element method (FEM) and integral equations (method of moments; MoM) for Maxwell equations solving. HFSS has a built-in automatic adaptive meshing that adjusts to each numerical model according to its size. A matrix is solved for every cell of the mesh at every point in a frequency sweep. This technology is called Mesh Fusion and thanks to its complex analysis of electromagnetic systems, real features of the designed elements can be predicted. [8]

Every antenna design itself requires a validation check (built-in function) before running an analysis. Passing the validation check is secured by setting up the correct conditions for the analysed structure. Besides the visual numerical 3D model of the antenna alone, its feeding technique, material and radiation area must be also defined. A frequency band for the analysis must be specified as well. Within this project, Ansys HFSS 2021 R2.2 was used.

2.2 Specific antenna requirements

2.2.1 Bandwidth

Considering information provided in chapter 1.1, a frequency band for the antenna can be computed. Centre frequency of the band f_c is given as arithmetic average of the sum of its limit centre frequencies f_{c_min} and f_{c_max}:

$$f_c = \frac{f_{c\_min}\ [\mathrm{MHz}] + f_{c\_max}[\mathrm{MHz}]}{2} = \frac{2402 + 2480}{2} = 2441\ \mathrm{MHz}\ . \qquad (2.1)$$

This will be needed for further calculations in the antenna design process described in following subchapters. An adequate impedance matching of the antenna

should be achieved in the whole BLE operation frequency band, meaning the return loss $|S_{11}| < -10$ dB within the band.

2.2.2 Substrate

In our application, material called Arlon 25N was used as the antenna substrate. It is publicly offered as a final product created by the Arlon Microwave Materials Division company. Parameters of the material can be found within the company's technical documentation. These must be considered when designing an antenna. [18]

Table 2.1 Substrate Arlon 25N parameters

Parameter	Symbol	Value	Unit
Thickness	h	1.524	mm
Relative permittivity	ε_r	3.38	-
Dielectric loss tangent	tan δ	0.0025	-

The substrate parameters significantly affect the excited wave parameters. Higher relative permittivity leads to wavelength shortening. Using another substrate would therefore require corresponding adjustments.

2.2.3 Antenna feeding technique

Antennas are commonly fed by SMA connectors with impedance $Z = 50\ \Omega$ connected to the electrical grid or a different source of electric energy. In the terms of planar antennas, this feeding technique can be accomplished by simply soldering a cable with SMA connector at its end onto the antenna's microstrip feedline. However, microstrips are very thin and could be a potential source of unwanted parasitic radiation. An antenna can be also fed by a coaxial probe. Realising this technique can be very challenging. The probe needs to be fixed in the antenna which involves holes drilling that can be considered a disadvantage.

Another planar antenna feeding method is a grounded coplanar waveguide (GCPW). This solution provides a good impedance matching and smaller power loss compared to microstrip. In our application, GCPW is used for all the designs excluding slot antenna.

In in the primary ANSYS HFFS designs, a lumped port is used as the wave excitation element. The port impedance is set to 50 Ω as it mimics the real cable connection.

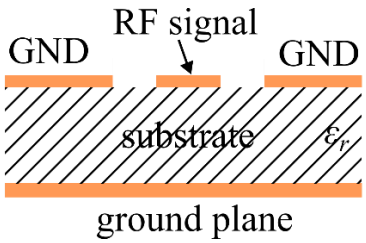

Fig. 2.1 Grounded coplanar waveguide (GCPW)

2.3 Suitable antennas overview

As suggested in the thesis introduction, planar antennas, fabricated via printed circuit board (PCB) technology, are used within this project. Small size, cheap price and easy, repeatable manufacture process, those are all advantages of this option. To achieve the desired antenna radiation, its shape must be defined. The scientific name for that shape is motif.

2.3.1 Planar wideband monopole

One of the chosen antenna motifs for BLE distance estimate is a wideband planar monopole. It is a variation of classic monopole where the arm is widened into a funnel. This layout simulates the shape of a standard wire monopole with a reflector.

Meanwhile the simplicity of this motif is considered an advantage, major limitation in the arm size adjustment can be viewed as a disadvantage. Parameters of the antenna are defined as the monopole width *W*, monopole length *L* and the GCPW dimensions. For visualisation, following figure may be used:

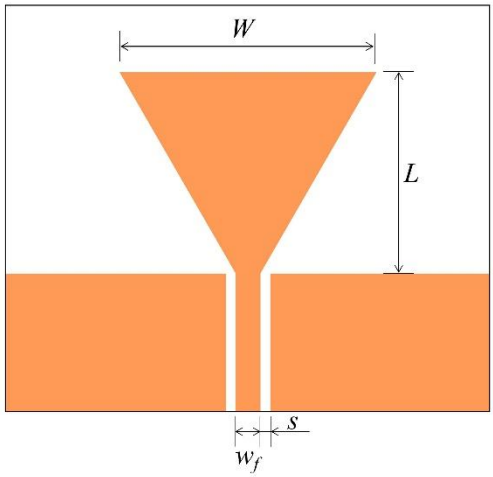

Fig. 2.2 Planar wideband monopole

Parameter w_f is width of the GCPW signal conductor. Parameter *s* corresponds to width of the gap between GCPW signal conductor and ground conductor.

By considering a quarter-wave planar wideband monopole, characteristics similar to half-wave dipole radiation can be achieved. The widened arm and the GCPW signal conductor together represent the monopole and both of the GCPW ground conductors imitate the reflector. Radiation of such antenna is omnidirectional excluding the direction of the arm axis, implying that the antenna may be applied vertically. Furthermore, linear polarization indicates the need of corresponding orientation of all the antennas used in communication with the monopole.

The length of the monopole *L* can be estimated as quarter of the wavelength using following formulas

$$\lambda = \frac{c}{f_c \cdot \sqrt{0.5(\varepsilon_r+1)}}, \tag{2.2}$$

where λ is the wavelength of the excited wave and

$$L = \frac{\lambda}{4} = \frac{c}{4f_c \cdot \sqrt{0.5(\varepsilon_r+1)}} = \frac{3 \cdot 10^8}{4 \cdot 2.441 \cdot 10^9 \cdot \sqrt{0.5(3.38+1)}} \doteq 20.8 \text{ mm} \quad , \tag{2.3}$$

where, in both cases, c is speed of light in vacuum, f_c is centre frequency of BLE operation band and ε_r is relative permittivity of the substrate.

Monopole width W affects the antenna input resistance. Experimentally, this parameter was set to $W = L/2 = 10.4$ mm. To complete the antenna design, parameters of the GCPW must be evaluated respecting the impedance matching and for these purposes, an online available calculator was used. [11] Considering the conductive layer thickness $T_{met} = 36$ µm and experimentally set GCPW parameters $w_f = 1.7$ mm and $s = 0.2$ mm, the calculator evaluates the characteristic impedance of transmission line as $Z_0 = 50.0462$ Ω. Therefore, sufficient impedance matching should be achieved using these parameters. The length of the GCPW was set to $L_{GCPW} = 15$ mm. For design simplification, the substrate was considered to be square shaped, and its dimensions were set to $G = 50$ mm. This substrate layout will be used among all suggested antenna models excluding sloth antenna (see 2.3.5). A numerical model with mentioned parameters was created in HFSS. [15]

The HFSS 3D antenna model can be found in the figure 2.3. By tuning the monopole arm L, resonant frequency, where the imaginary part of input impedance is zero, is changed. The higher set value of L, the lower resonant frequency is obtained. Hence, using this knowledge, the impedance matching can be achieved throughout the whole BLE band. Tuned parameters for the wideband monopole are presented in the table 2.2.

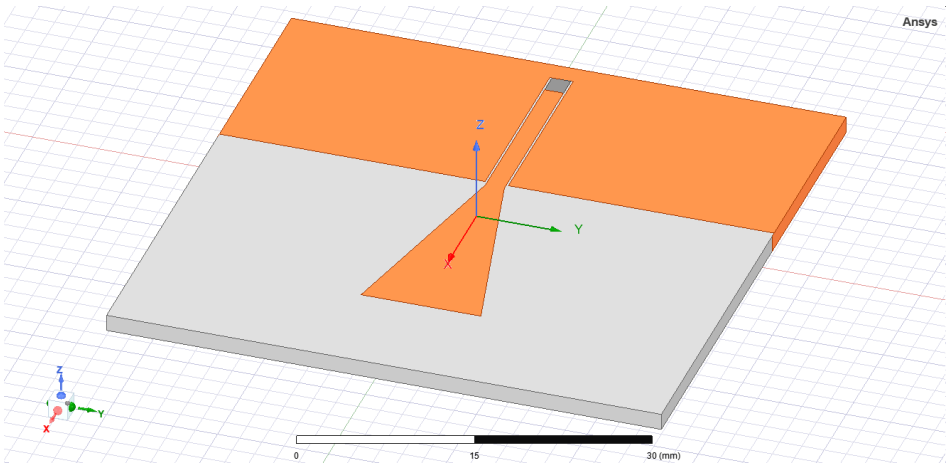

Fig. 2.3 HFSS planar wideband monopole 3D model

Table 2.2 Planar wideband monopole 3D model parameters

Symbol	Description	Value	Unit
L_{GCPW}	coplanar waveguide length	15.5	mm
s	gap between GCPW conductors	0.2	mm
w_f	GCPW signal conductor width	1.7	mm
L	monopole length	20.2	mm
W	monopole width	10.2	mm

The antenna return loss is shown in figure 2.4. The return loss condition $|S_{11}| < -10$ dB is clearly met within the whole operation band and therefore, the impedance matching is done correctly.

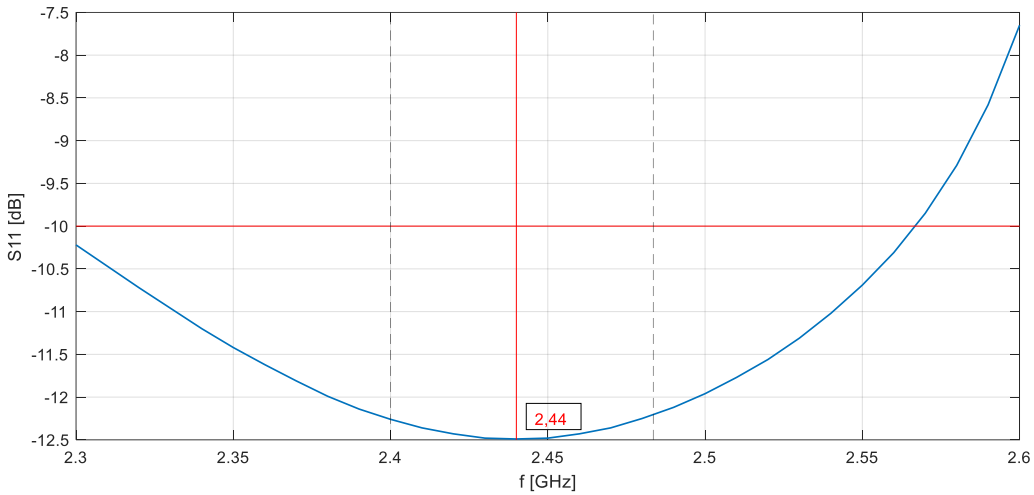

Fig. 2.4 Wideband planar monopole return loss S_{11}

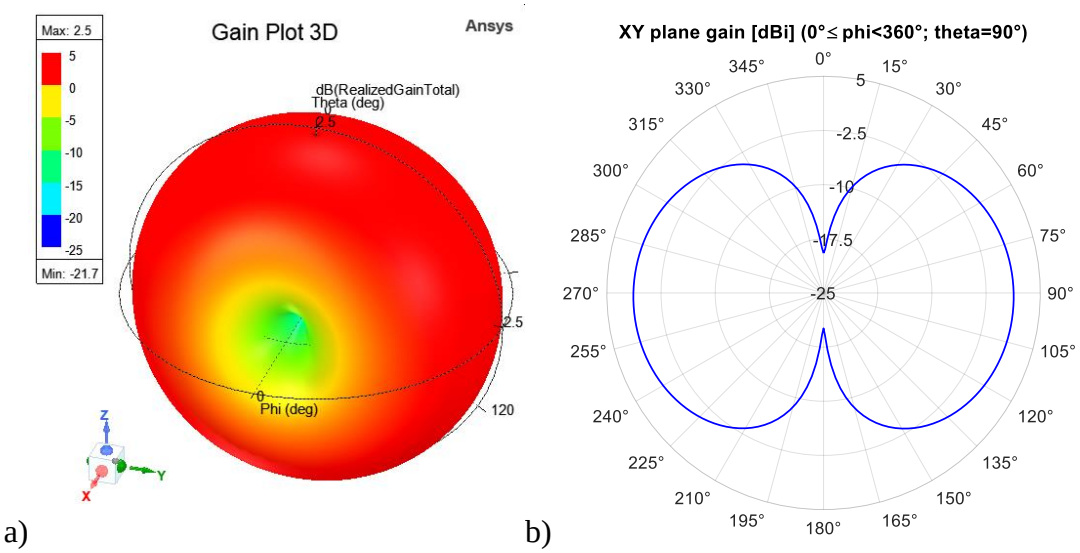

a) b)

Fig. 2.5 Radiation pattern at 2.44 GHz a) 3D, b) in XY plane (H-plane)

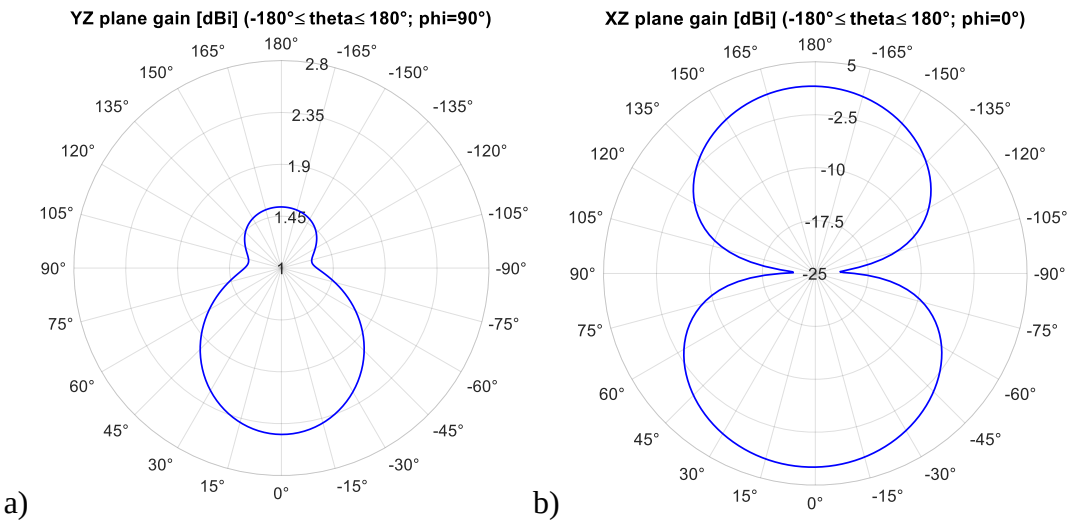

a) b)

Fig. 2.6 Radiation pattern at 2.44 GHz in a) YZ plane b) XZ plane (E-planes)

The radiation patterns at BLE centre frequency (which is also the resonant frequency in this case) in figures 2.5 and 2.6 show that the wideband planar monopole truly radiates precisely as a half-wave dipole does. This antenna is omnidirectional excluding the direction of the monopole axis where the radiation is at its minimum. In the terms of spherical coordinate system, minimal radiation is obtained when $\varphi = 0°$ and $\varphi = 180°$ in XY plane and when $\theta = 90°$ and $\theta = -90°$ in XZ plane.

Realised gain of the antenna was evaluated in HFSS when plotting the antenna 3D radiation pattern and its value is $G = 2.5$ dB at frequency 2.44 GHz as shown in figure 2.5a). For a better impedance matching, an impedance transformer would have to be additionally considered in the GCPW motif.

2.3.2 Planar L-shaped monopole

Another motif for a small antenna is a planar L-shaped monopole. The arm of the monopole is bent, and it takes a 90-degree turn to form a shape similar to the letter “L”. By bending the monopole, a lot of space on the substrate can be saved since a standard monopole would require bigger substrate dimensions.

Parameters of this antenna are defined as bent monopole arm width W, bent monopole arm length L and GCPW parameters which stay the same as in the wideband monopole model (chapter 2.3.1), meaning w_f is, again, GCPW signal conductor width as well as s is the size of the gap between GCPW conductors. Additionally, a parameter *offset* is presented as the space between the bent arm and ground. For better layout visualisation, following figure may be used:

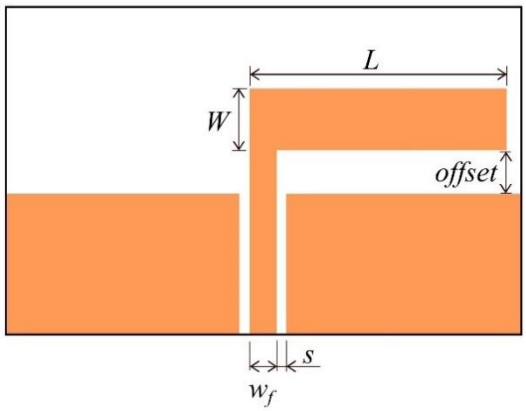

Fig. 2.7 Planar L-shaped monopole

L-antenna dimensions estimate can be evaluated using the same approach used for the previous monopole. The initial parameters setup is therefore very similar to the previously presented one. Considering a quarter-wave antenna again, the equation (2.3) can be used and hence, the bent monopole arm length L is set to 20.8 mm. To effectively utilize the space on the substrate, the gap between the arm and the ground is set to $offset = L/5 = = 4.2$ mm. Since the arm is basically an elongated GCPW signal conductor, its width should correspond to the w_f parameter. However, wider monopoles are more mechanically robust and have a wider range of frequencies within which a good impedance matching can be achieved. Therefore, the parameter W was experimentally set to $W = 3$ mm. [15]

GCPW and substrate dimensions remain unchanged. All the parameters used for the adjusted version of this antenna can be found in table 2.3.

Table 2.3 Planar wideband monopole 3D model parameters

Symbol	Description	Value	Unit
L_{GCPW}	coplanar waveguide length	19.6	mm
s	gap between GCPW conductors	0.2	mm
w_f	GCPW signal conductor width	1.7	mm
L	length of the bent monopole arm	18.8	mm
W	width of the bent monopole arm	2.7	mm
$offset$	gap between the bent arm and GND	3.7	mm

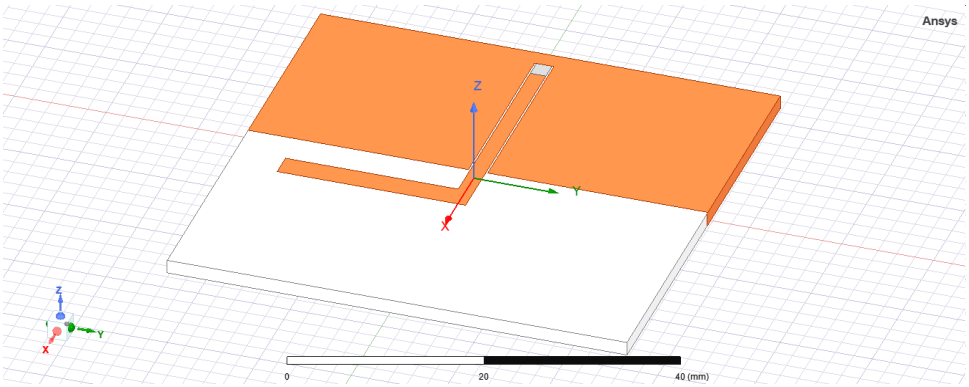

Fig. 2.8 HFSS planar L-shaped monopole 3D model

Figure 2.8 proves that the L-shaped monopole utilizes the space on the substrate very effectively. According to antenna theory, this monopole is considered a short antenna which input impedance has a dominant capacitive part. To compensate this reactance, a short-ended shunt may be used. However, this procedure would create a different motif, a planar inverted F antenna (PIFA, see 2.3.3).

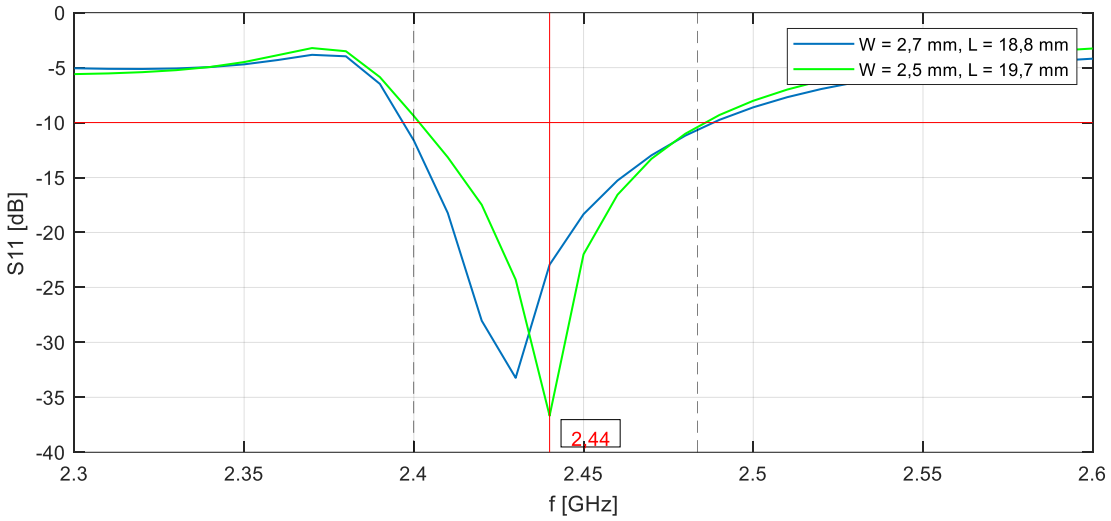

Fig. 2.9 Planar L-shaped monopole return loss S_{11}

From the information provided in figure 2.9, the antenna with parameters W = 2.7 mm and L = 18.8 mm can be declared as correctly set up. Thus, the monopole's impedance matching is well done within the entire BLE band. However, its centre frequency is not at 2.44 GHz but rather at frequency 2.43 GHz meaning the imaginary part of input impedance is not zero at the BLE centre frequency. By changing the antenna parameters to W = 2.5 mm and L = 19.7 mm, the resonant frequency shifts to 2.44 GHz at the cost of not achieving the condition $|S_{11}| < -10$ dB within the whole BLE band. That means that at the most left side of the BLE band, more than 10 % of the radiated energy would be reflected into the antenna input.

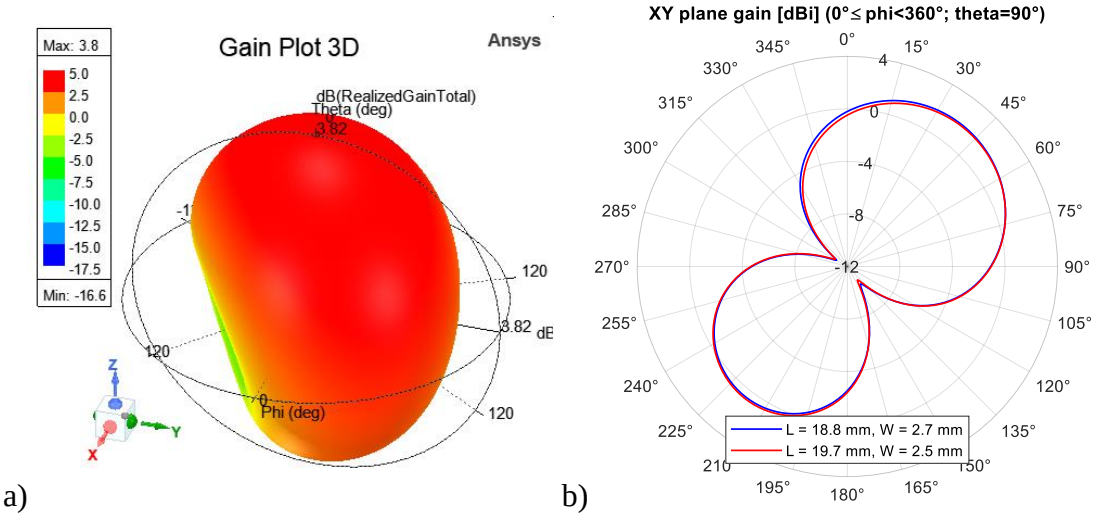

Fig. 2.10 Radiation pattern at 2.44 GHz a) 3D, b) in XY plane (H-plane)

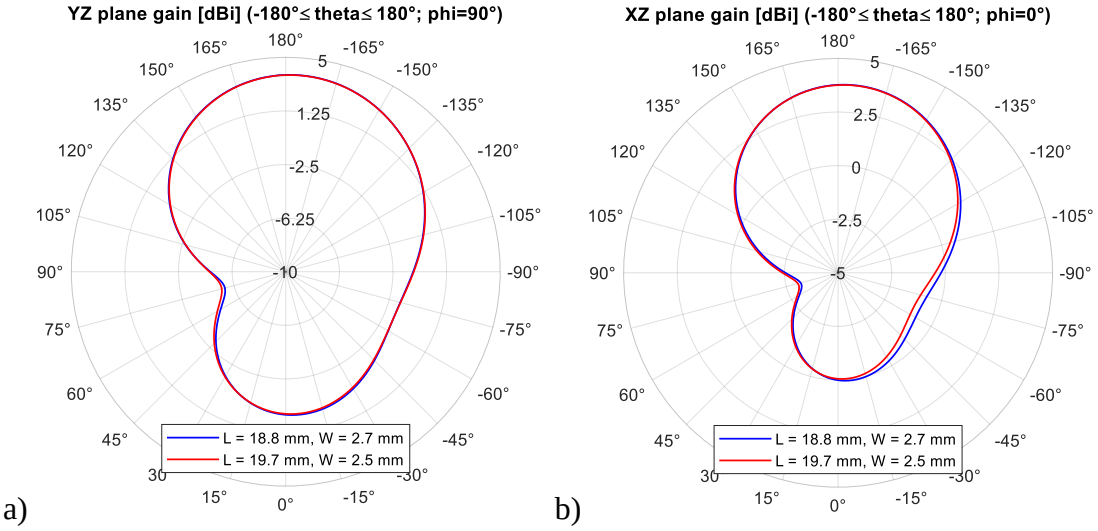

Fig. 2.11 Radiation pattern at 2.44 GHz in a) YZ plane b) XZ plane (E-planes)

Figure 2.10a) is shown from the same point of view as the 3D antenna model in figure 2.8. Therefore, a better visualisation of the antenna spatial radiation can be obtained. In the figures 2.10 and 2.11 it is shown that a slight change of the parameters does not significantly affect the radiation pattern. The antenna gain for frequency 2.44 GHz was evaluated by HFSS as G = 3.8 dB. According to figure 2.11, the gain was measured in the E-planes (planes YZ and XZ) in the direction of theta θ = -180°.

2.3.3 Planar inverted F antenna (PIFA)

As mentioned in the previous subchapter, PIFA is, in fact, a printed monopole antenna which arm is bent, and which has an additional short-ended shunt. This shunt creates an antenna motif that is shaped like an inverted "F" letter.

Dimensions of this antenna can be defined as width of its bent arm *W*, length of the bent arm *L*, length of the short-ended shunt L_P, the distance between the bent arm and ground *offset* a GCPW parameters. For better visualisation, use:

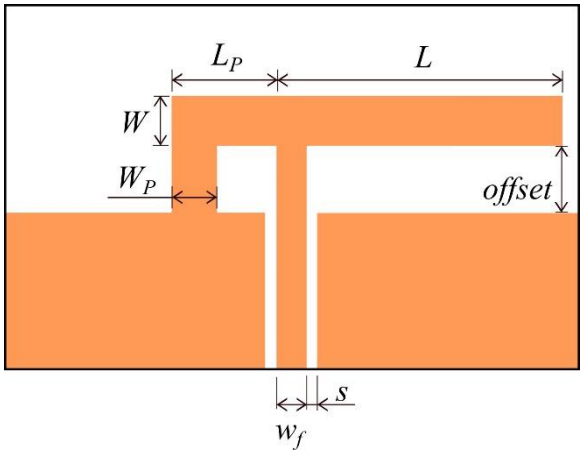

Fig. 2.12 PIFA

Parameters w_f and *s* are the GCPW dimensions and W_P represents the width of the shunt to ground conductive connection.

The default parameters were acquired from the previous L-antenna model in subchapter 2.3.2 and the shunt dimensions were experimentally set up to L_P = 3 mm and W_P = *W* = 3 mm. Simulations were made and the antenna parameters were accordingly tuned. Their values can be found within the table 2.4.

Table 2.4 PIFA 3D model parameters

Symbol	Description	Value	Unit
L_{GCPW}	coplanar waveguide length	19.3	mm
s	gap between GCPW conductors	0.2	mm
w_f	GCPW signal conductor width	1.7	mm
L	length of the bent arm	12.1	mm
W	width of the bent arm	2	mm
offset	gap between the bent arm and GND	2.7	mm
W_p	width of the shunt-GND connection	2	mm
L_p	length of the short-ended shunt	3.8	mm

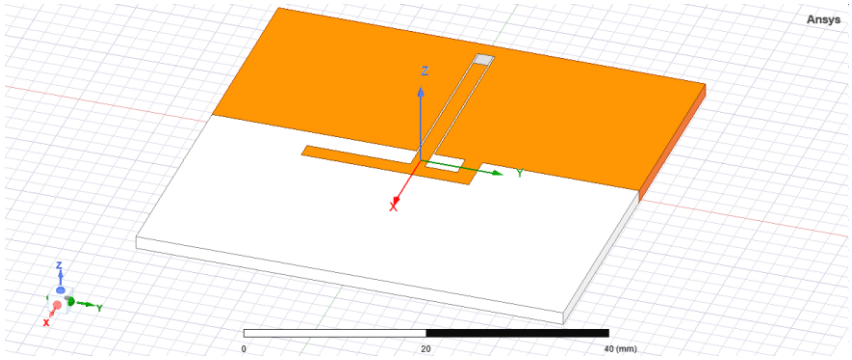

Fig. 2.13 HFSS PIFA 3D model

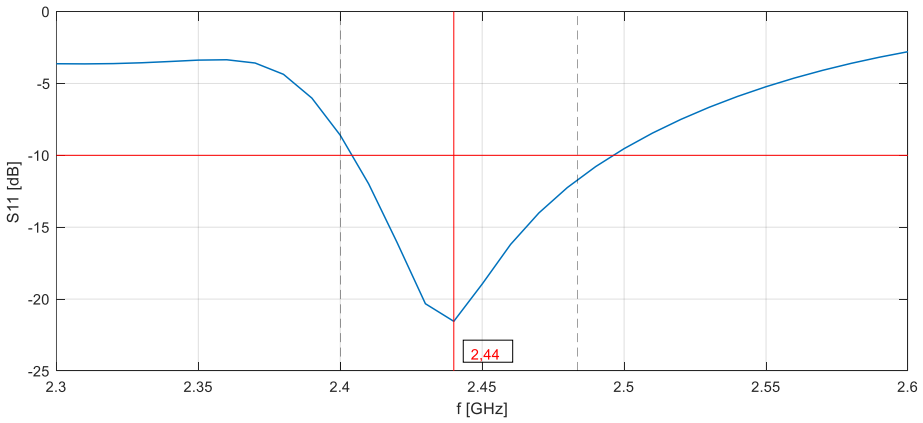

Fig. 2.14 PIFA return loss S_{11}

Figure 2.14 shows that the impedance matching is not achieved within the whole BLE operation band. At the start frequency 2.4 GHz, return loss S_{11} is only -8.57 dB. On the other hand, a good impedance matching Z_a = (47.76 + j7.9) Ω is obtained at the resonant frequency 2.44 GHz.

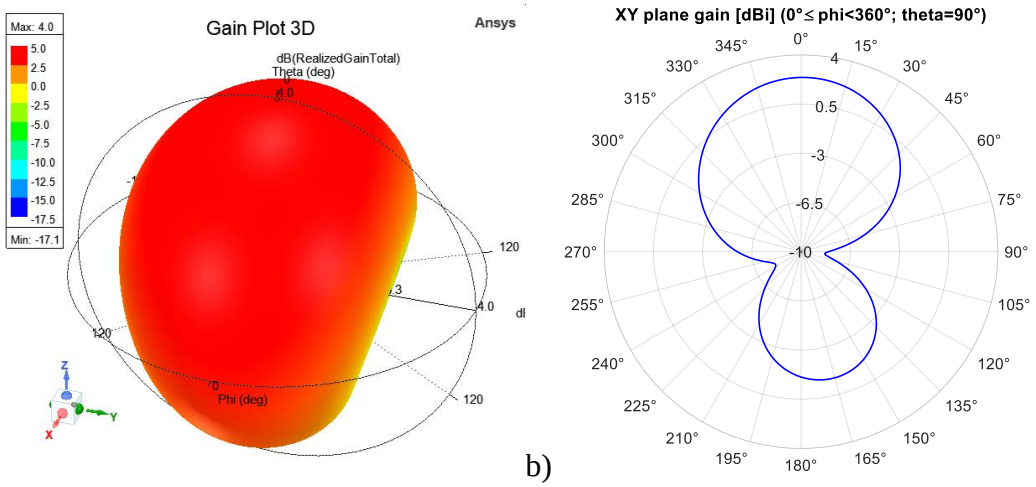

a) b)

Fig. 2.15 Radiation pattern at 2.44 GHz a) 3D, b) in XY plane (H-plane)

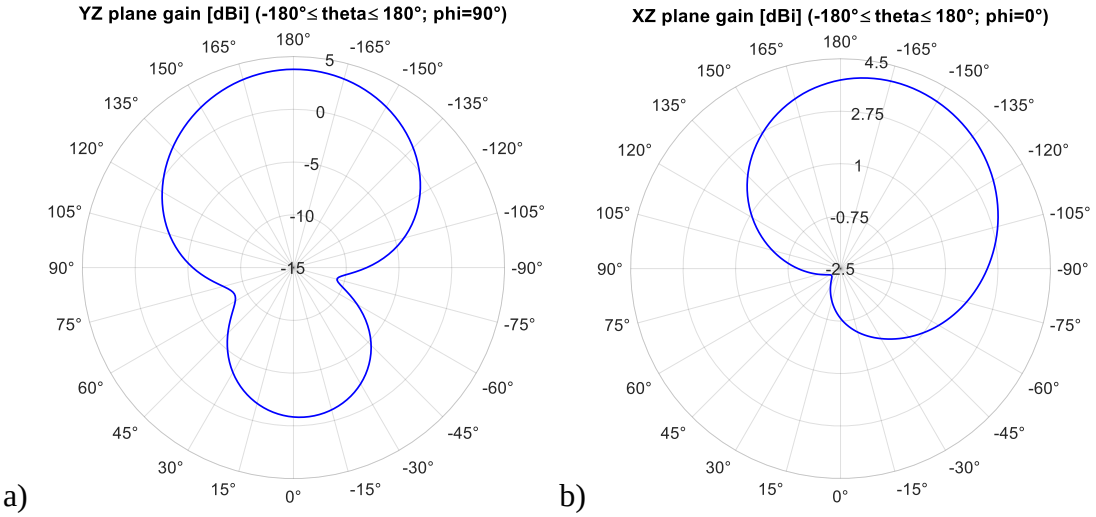

a) b)

Fig. 2.16 Radiation pattern at 2.44 GHz in a) YZ plane b) XZ plane (E-planes)

According to figures 2.15 and 2.16, gain of this antenna model has the highest value among all the up to now created antennas. However, its radiation pattern was significantly reduced. This reduction is caused by the shunt's presence, and it can be found XZ plane when theta ϑ = 45° as shown in figure 2.16b). In the opposite direction, ϑ = -155°, the antenna gain G = 4 dB can be found.

2.3.4 Meander antenna

The fourth suggested antenna motif is another modification of a monopole. This antenna maximally utilizes the space available on substrate by folding the monopole arm into meanders. A big scale of design parameters modification is obtained, although the complexity of creating such antenna can be very challenging.

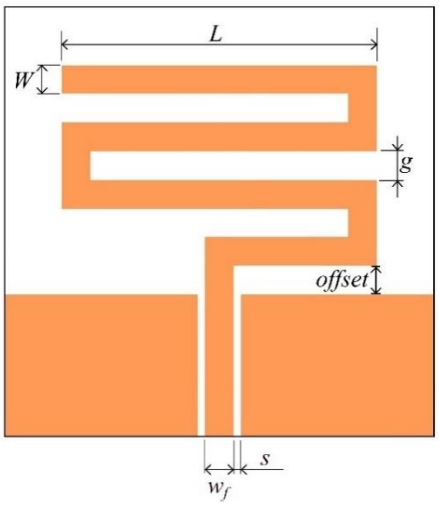

Fig. 2.17 Meander antenna

Dimensions of meander antennas can be defined by meander line width W, meander line length L, size of the gap between meander lines g and GCPW parameters w_f and s.

Additionally, *offset* is the distance between the first meander line and ground. For better visualisation, following figure may be used. Total length of the monopole is now divided into multiple segments that fit into much smaller substrate dimensions than a standard monopole would. To provide more flexibility when designing an antenna, an open-ended shunt is added to the meander motif. The shunt compensates the antenna input reactance. Resonant frequency can be tuned by changing the last meander line length.

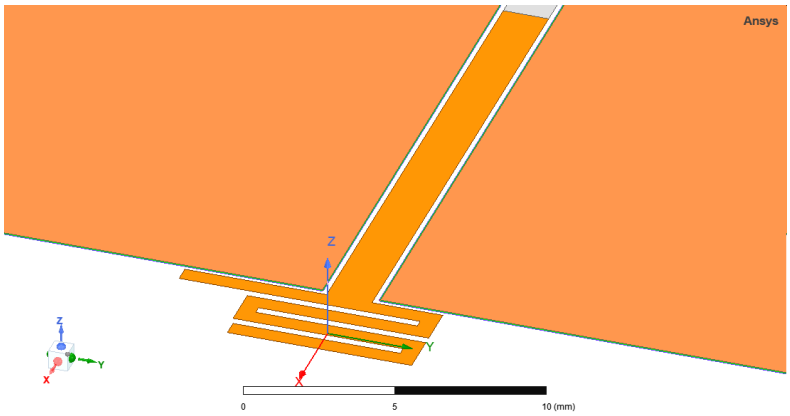

Fig. 2.18 HFSS meander antenna 3D model

Table 2.5 Meander antenna 3D model parameters

Symbol	Description	Value	Unit
L_{GCPW}	coplanar waveguide length	18.5	mm
s	gap between GCPW conductors	0.2	mm
w_f	GCPW signal conductor width	1.6	mm
L	meander line length	6.6	mm
W	meander line width	0.6	mm
g	gap between meander lines	0.3	mm
offset	gap between the first meander line and GND	0.1	mm
P	open shunt length	2.5	mm
end	shortage of the last meander line	2.6	mm

Meander monopole parameters can be found within the table 2.5. The antenna radiation is shown in figures 2.20 and 2.21. Antenna input impedance at the resonant frequency 2.44 GHz is Z_a = (44,76 - j6.21) Ω which can be considered as good impedance matching. The main radiation lobe of the meander antenna is in the XZ plane (E-plane) when theta is at -180° and the gain obtained here is G = 0.9 dB.

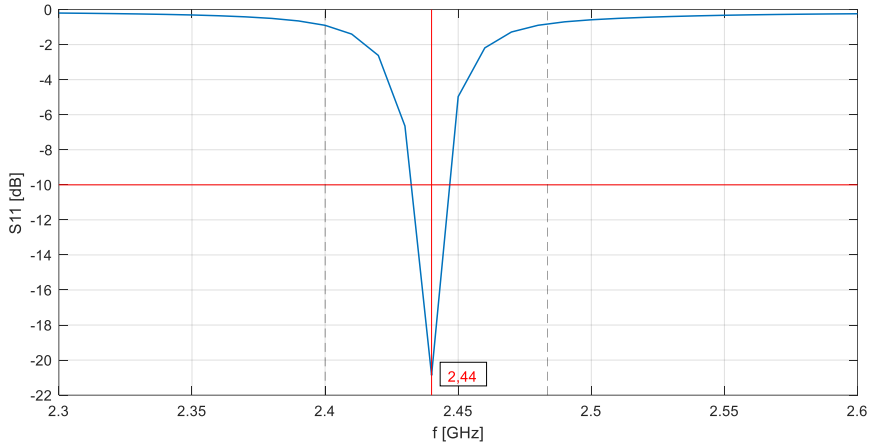

Fig. 2.19 Meander antenna return loss S_{11}

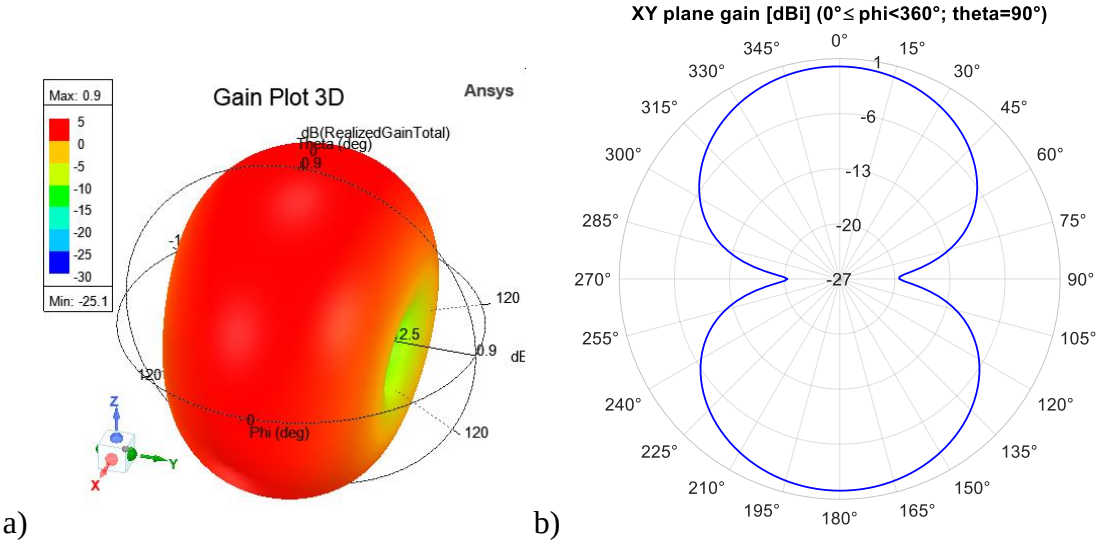

a) b)

Fig. 2.20 Radiation pattern at 2.44 GHz a) 3D, b) in XY plane (H-plane)

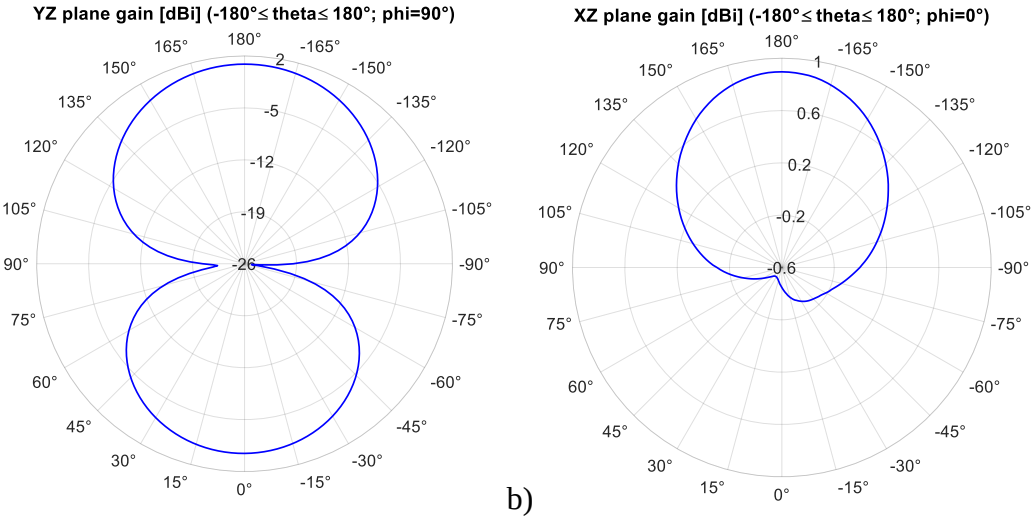

a) b)

Fig. 2.21 Radiation pattern at 2.44 GHz in a) YZ plane b) XZ plane (E-planes)

2.3.5 Slot bow tie antenna

The last chosen motif is a slot bow tie antenna. More detailed description of this concept can be found in [17]. As the primary step of the design process, a basic bow tie slot dipole antenna is created. This default setting is considered the zeroth iteration. To save space, the dipole arms are serrated. Every additional serration is considered an *n*-th iteration, where *n* represents the number of serrations. The principle of this process is shown in the figure below:

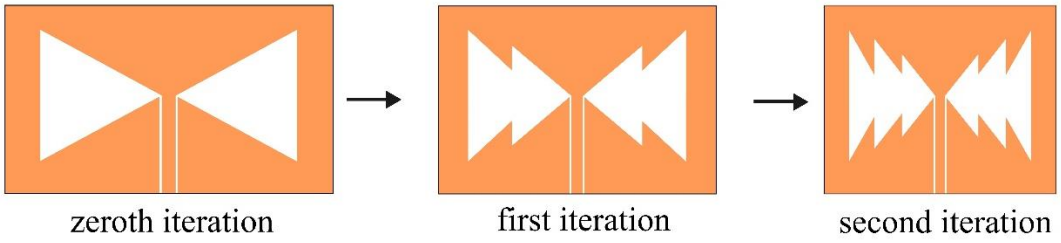

Fig. 2.22 Iteration procedure

Instead of GCPW feeding technique, coplanar waveguide (CPW) is used creating a possibility to have only one conductive layered antenna. However, this set up causes a DC short circuit in antenna, making it electrically small. These kinds of antennas are known to have a radiation pattern similar to radiation of a dipole and are considered magnetic dipoles. [17]

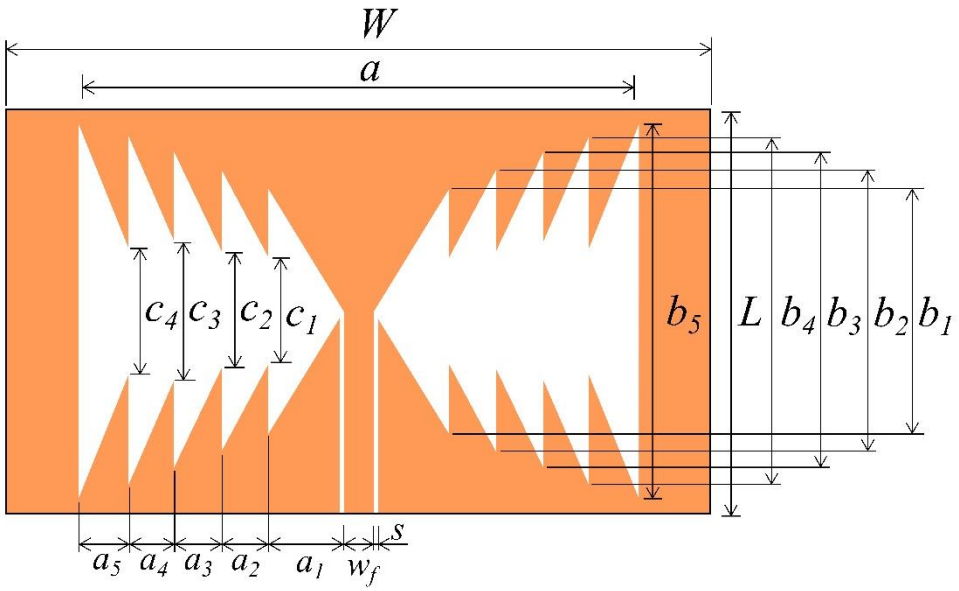

Fig. 2.23 Slot bow tie antenna

Antenna design dimension can be seen above. The core antenna parameters are its width *W* and length *L*. The arms, which are symmetrical to each other respecting the longitudinal axis, are divided to individual regions with widths a_1-a_5, lengths c_1-c_4 on the shorter side and lengths b_1-b_5 on the longer side. Finally, w_f and *s* are the CPW dimensions.

Using the following formula, where n is the number of iterations, all the region widths a_1-a_5 can be computed:

$$\sum_{k=0}^{n} a_k = \frac{(a-2s-w_f)}{2(n+1)} = \frac{(27.6-2\cdot 0.2-1.6)}{2\cdot(4+1)} = 2.56 \text{ mm} \quad . \tag{2.4}$$

Region lengths were considered even $c_1 = c_2 = c_3 = c_4 = 2$ mm. Thus, Final parameters of the designed antenna are listed in the table 2.6.

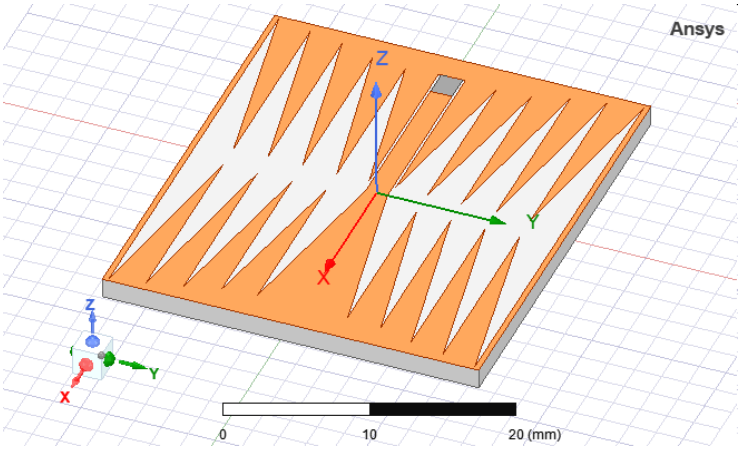

Fig. 2.24 HFSS slot bowtie antenna 3D model

Table 2.6 Slot bow tie antenna 3D model parameters

Symbol	Description	Value	Unit
L	substrate length	32	mm
W	substrate width	28	mm
L_{GCPW}	coplanar waveguide length	16	mm
s	gap between CPW conductors	0.2	mm
w_f	CPW signal conductor width	1.6	mm
a	arm end to arm end distance	27.6	mm
a_1-a_5	region widths	2.56	mm
c_1-c_4	regions shorter side lengths	2	mm
$b1$	first (most inner) region longer side length	27.5	mm
$b2$	second region longer side length	28	mm
$b3$	third region longer side length	29.5	mm
$b4$	fourth region longer side length	30.5	mm
$b5$	fifth (most outer) region longer side length	31.5	mm

As shown in figure 2.25, impedance matching condition is satisfied throughout the whole BLE band. The antenna radiates like a half-wave dipole and its gain in YZ plane was evaluated by HFFS as $G = 2.6$ dB.

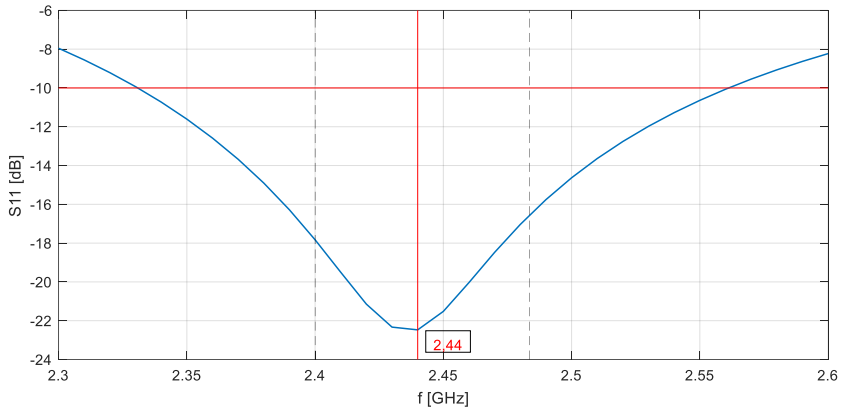

Fig. 2.25 Slot bow tie antenna return loss S_{11}

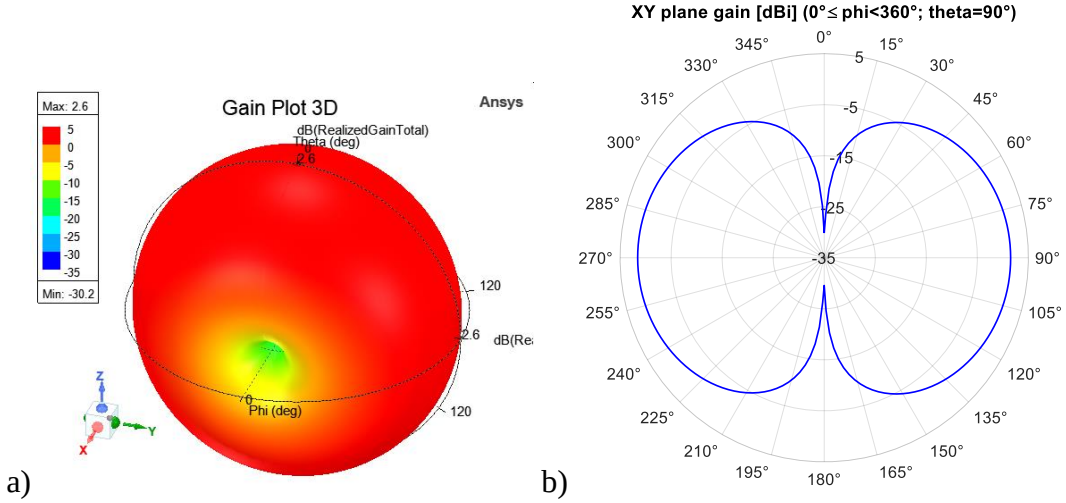

a) b)

Fig. 2.26 Radiation pattern at 2.44 GHz a) 3D, b) in XY plane (E-plane)

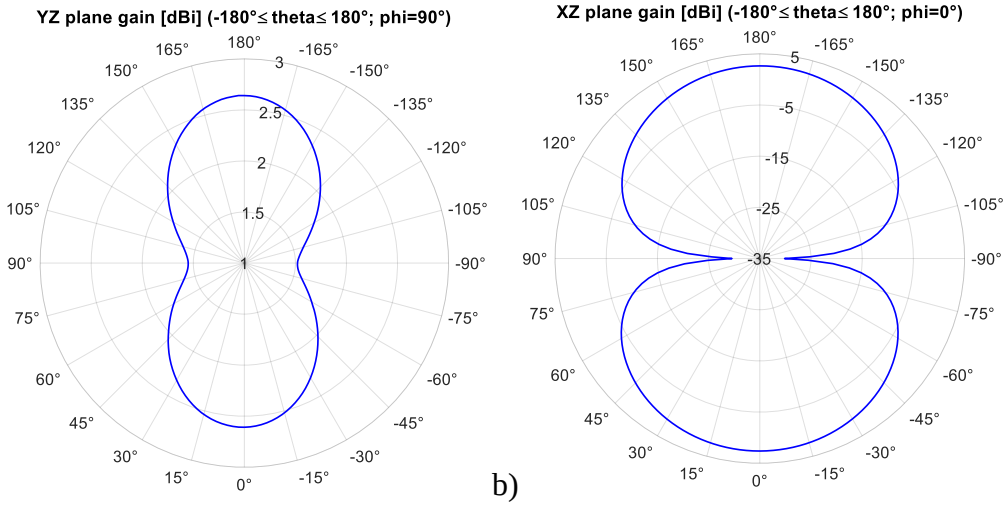

a) b)

Fig. 2.27 Radiation pattern at 2.44 GHz in a) YZ plane b) XZ plane (H-planes)

3. ANTENNAS COMPARISON

Within this chapter, all the designed antenna models are discussed taking three different factors into account. Regarding our application, every aspect is considered equally important.

3.1 Return loss (S_{11} parameter)

All models' frequency sweep return loss is plotted in figure 3.1. Within the black marked operating band, wideband monopole, L-shaped antenna and slot antenna achieved the impedance matching condition. However, resonant frequency of L antenna is not at the BLE band centre frequency and the wideband monopole could achieve better impedance matching by adding a transformer into its motif.

Although PIFA does not satisfy the required impedance matching within the desired band, most of its bandwidth covers the condition $|S_{11}| < -10$ dB. Meander antenna impedance matching is correctly done only at centre of the operation band and thus it cannot be considered a suitable antenna for our application in the terms of return loss.

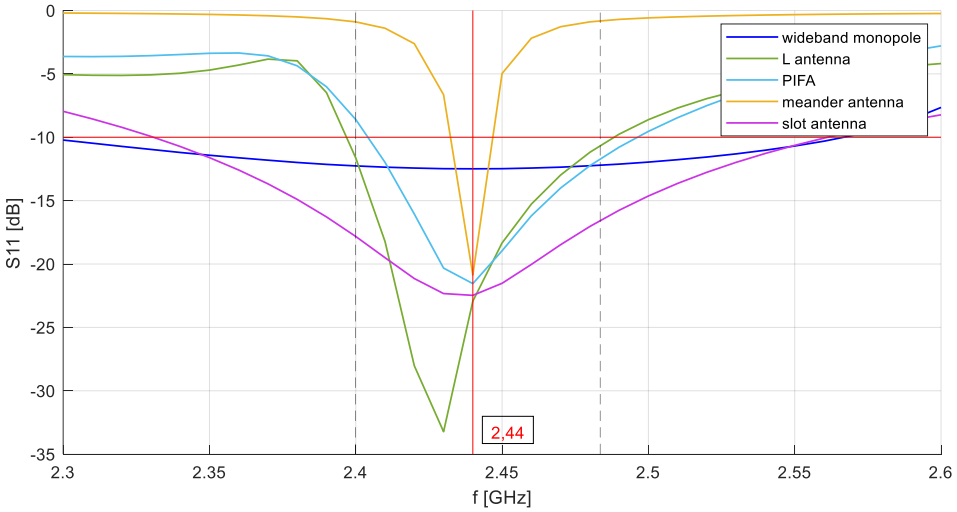

Fig. 3.1 All models' return loss S_{11}

3.2 Radiation pattern and gain

Both planes radiation patterns of all the designed antennas at frequency 2.44 GHz can be found in figures 3.2 and 3.3. The colour legend is adjusted to all models return loss comparison in 3.1 above, meaning dark blue line is the wideband monopole characteristic et cetera.

In XY plane, none of the considered antennas radiation is omnidirectional. On the other hand, omnidirectionality is achieved within the other planes. Wideband monopole and slot antenna show that kind of radiation in YZ plane. L antenna and PIFA have

a radiation drop in direction of the bent arm in case of L antenna and in direction of the shunt and bent arm in case of PIFA which is more visible in the figure 3.4. Meander antenna can be considered omnidirectional in XZ plane. This comparison provides a proof that antenna spatial orientation is important.

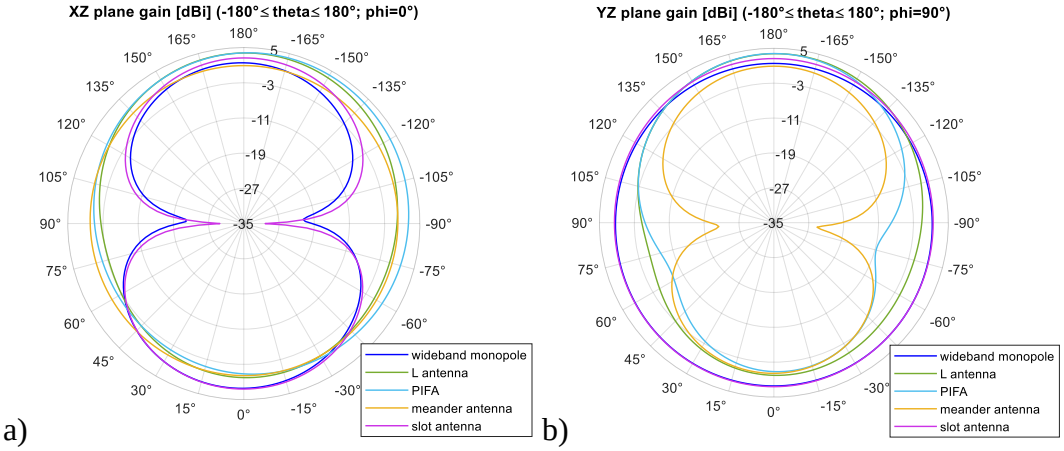

a) b)

Fig. 3.2 All models' radiation patterns at 2.44 GHz in a) XZ plane b) YZ plane

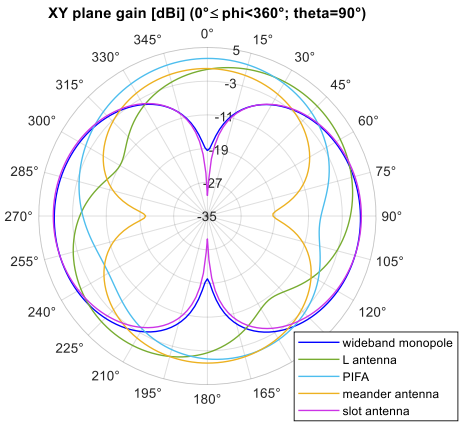

Fig. 3.3 All models' radiation patterns at 2.44 GHz in XY plane

Antenna radiation patterns are closely related to its gain. The HFSS program computed those values for all the models and each gain is listed in the table 3.1. Since wideband monopole and slot antenna radiate like a standard dipole, their gains $G_{\text{wideband\_monopole}}$ = 2.5 dB and $G_{\text{slot\_antenna}}$ = 2.6 dB are similar to each other due to considering the same excitation method. L antenna and PIFA gains $G_{\text{L\_antenna}}$ = 3.8 dB and G_{PIFA} = 4 dB are the highest among all the models because they both are not omnidirectional in any direction. Demonstration of the radiation power loss can be seen in the figure below.

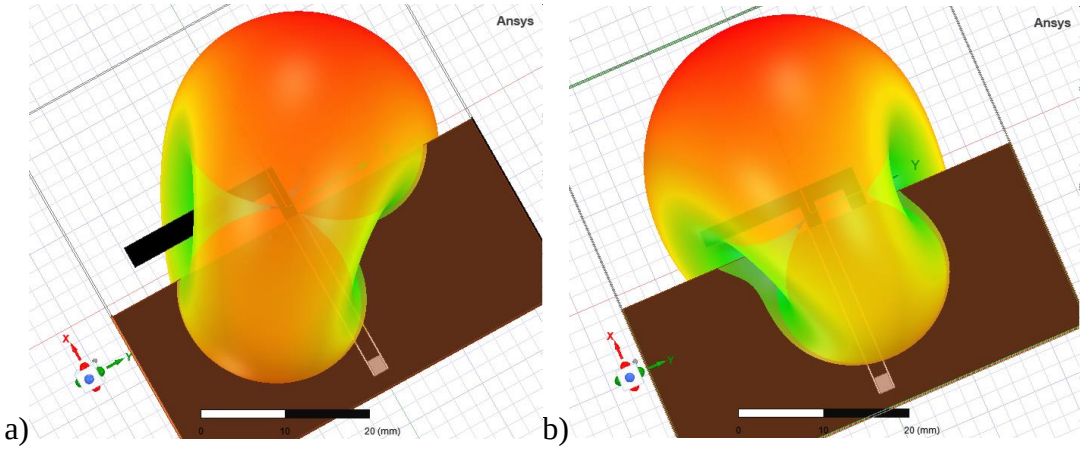

Fig. 3.4 3D radiation patterns at 2.44 GHz of a) L antenna b) PIFA

3.3 Antenna size

Since the substrates of all models, excluding slot antenna, were square shaped with dimensions 50 mm × 50 mm, total sizes of the four first models are equal. However, in the terms of motif size on substrate alone, the most space saving antenna is meander antenna. Its motif has 3.4 mm in the GCPW direction, and the antenna's total longitudinal size is 21.9 mm. In the latitudinal direction, it has 9.1 mm. Both PIFA and L antenna have quite hight potential of space saving, whereas PIFA is slightly smaller than L antenna. Considering the format X × Y where X is the length with GCPW and Y is the motif width, PIFA size is 24 mm × 15.9 mm and L antenna size is 26 mm × 18.8 mm. Wideband planar monopole occupies the most space and its motif size is 35.7 mm × 10.2 mm. Finally, slot antenna size is equal to its substrate size 32 mm × 28 mm, making it the smallest antenna among all the suggested models.

However, all models' sizes are within the considered substrate dimensions and can be adjusted to a smaller substrate depending on the space saving potential. The adjustment was not made for most of the models to observe that potential. In the case of slot antenna, the size had to be adjusted along with the iteration level and thus its dimensions differ.

3.4 Summary

Comparison across all the mentioned aspects was made and the summarization can be found in the table 3.1. In the terms of frequency band within which impedance matching is done correctly, wideband planar monopole has the biggest bandwidth as it could have been predicted from its name. Considering antenna gain, the best solutions would be PIFA or L antenna. However, both antennas are not omnidirectional, and our application requires an omnidirectional antenna since it consists of position and distance estimating. Despite having the best space saving potential, meander antenna cannot be evaluated as a suitable option. The design did not achieve the impedance matching condition within

the whole BLE band. As a compromise considering all the given information, slot bowtie antenna was chosen to be optimized and further analysed.

Table 3.1 All models summarization

Model	Bandwidth	Gain	Motif size
wideband monopole	2.290 – 2.650 GHz	2.5 dB	35.7 mm × 10.2 mm
L antenna	2.395 – 2.485 GHz	3.8 dB	26.0 mm × 18.8 mm
PIFA	2.409 – 2.483 GHz	4.0 dB	24.0 mm × 15.9 mm
meander antenna	2.431 – 2.446 GHz	0.9 dB	21.9 mm × 9.1 mm
slot bow tie antenna	2.331 – 2.560 GHz	2.6 dB	32.0 mm × 28.0 mm

4. ANTENNA OPTIMIZATION

To optimize the chosen antenna for NXP KW45 chip described in chapter 1.3, an SMA connector is to be implied within the 3D numerical model. Considering the application, the car key fob and human impact should be included into the design process.

4.1 SMA connector

Nowadays electronic components market offers a very large scale of products including various types of SMA connectors. These connectors vary in size, but their impedance is always adjusted to $Z_{SMA} = 50\ \Omega$. Since the antenna model was created and analysed using lumped port with impedance 50 Ω in HFFS, changing the excitation method will affect the model radiation. The conductive strip at the antenna input needed for lumped port usage is removed which creates a resonant frequency shift and additionally, the input impedance decreases.

Considering the SMA dimensions mentioned in [10], a 3D model of it was created and added to the antenna model. Two conductive objects (dark grey in the figure 4.1) were constructed within the design according to the soldering technique described in [7]. Adding a conductive link between the coplanar waveguide ground conductors and the flange did not affect the model and thus it was removed and not considered. Maintaining the overall antenna size, the slot motif was adjusted to compensate the removed strip. Only tuned parameters are listed in the table 4.1.

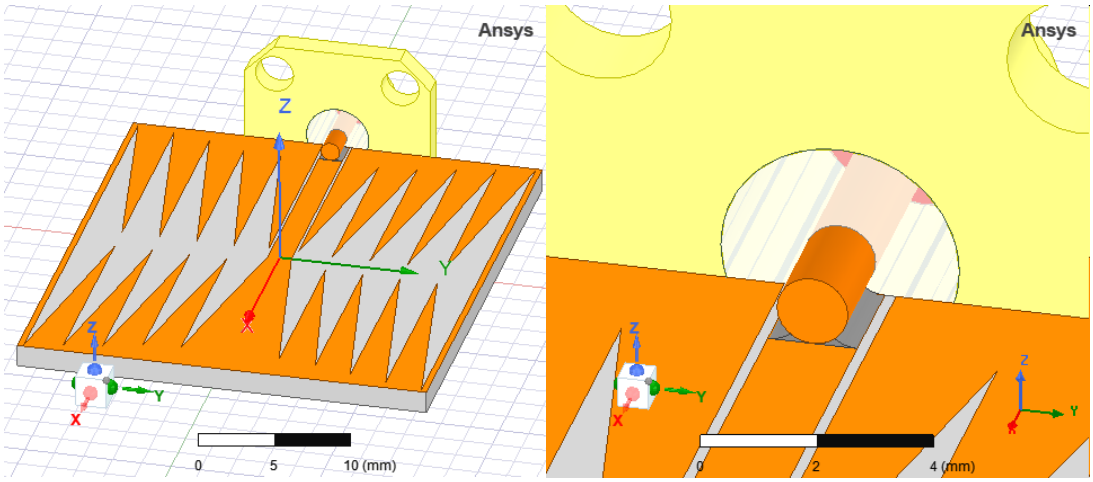

Fig. 4.1 Slot bow tie antenna with SMA connector and zoomed in point of view

As shown in figure 4.2, after adding the SMA connector model into the primary design, the antenna parameters needed to be adjusted as the impedance matching condition was completely missed within the operation band. Tuning the motif inner dimensions resulted into achieving a good impedance matching again.

Table 4.1 Adjusted slot bow tie antenna 3D model parameters

Symbol	Description	Value	Unit
s	gap between CPW conductors	0.3	mm
w_f	CPW signal conductor width	1.5	mm
c_1-c_4	regions shorter side lengths	0.8	mm
b1	first (most inner) region longer side length	28	mm
b2	second region longer side length	29	mm
b3	third region longer side length	30.5	mm
b4	fourth region longer side length	31	mm
b5	fifth (most outer) region longer side length	31.5	mm

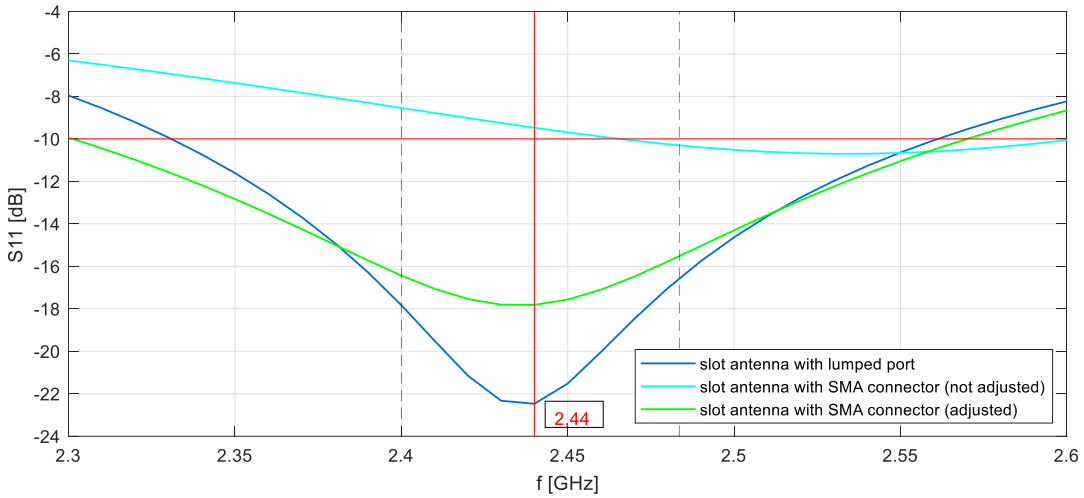

Fig. 4.2 Slot bow tie antenna with SMA return loss S_{11}

4.2 Car key fob

Designing an antenna implementable into a car key fob requires consideration of the fob's influence on the antenna radiation within the process. Today's automotive industry has a very diverse offer of car keys. Key fobs both with and without a mechanical metallic key are available.

The manufactured antenna was not optimized for any key fob due to the base of our application and unavailability of the fob itself. Having the antenna inside of a cover would also require drilling a hole into that cover as the NXP KW45 is structured to be used with a device with SMA connector.

4.3 Human impact

The human presence in antenna's near-field has a big impact on its radiation. To examine the influence, human tissue characteristics is unified, and its presence is substituted by phantoms. In simulations, numerical phantoms are used. The only two disadvantages of this human tissue substitute are the complexity of the body modelling process and the complicated evaluation process which can be very challenging for the computer processor. Thus, in many cases, only simplified layers of the tissue are created in the simulator. [20]

When analysing real life situations, physical phantoms which are adjusted to the analysed frequency must be used. In our application, a one-layer agar phantom with dimensions 145 mm x 145 mm x 33 mm is applied. Its permittivity is $\varepsilon_r = 50$ and specific electrical conductivity $\sigma = 7.5$ S/m.

Phantoms generally have high relative permittivity which causes a big shift in the antenna's bandwidth. To demonstrate the impact on antenna's radiation, a numerical phantom model with an 8mm gap from the antenna's backside was created in HFSS. Later, a physical phantom with the same parameters will be used experimentally in real antenna measurements (see chapter 5).

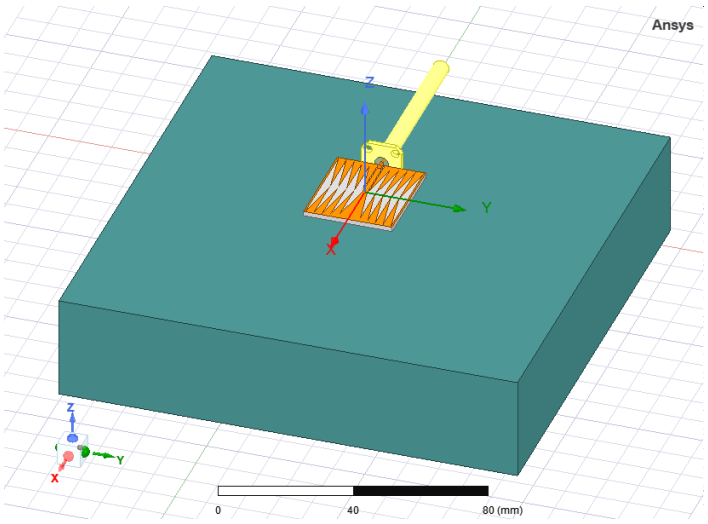

Fig. 4.3 HFSS slot bow tie antenna 3D model with phantom

Different phantom parameters substituting different human bodies would show slightly different results. The antenna was not optimized for human tissue regarding the complexity and expensiveness of a precise physical phantom creating process which was not the object of this study.

5. EXPERIMENTAL ANTENNA MEASUREMENTS

Within this chapter, analysis of the real manufactured antenna is provided by measuring its return loss and radiation pattern. The phantom impact described in 4.3 is demonstrated. Antenna radiation is measured in an anechoic chamber. Experimental measurements in real environment are presented. All the measurements were made specifically in the Faculty of Electrical Engineering and Communication in Brno.

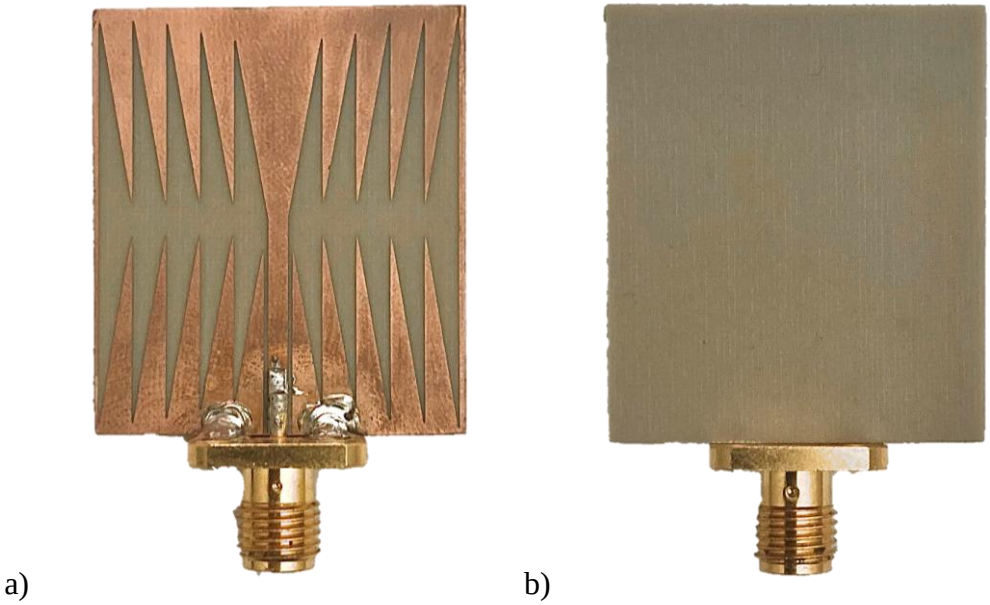

a) b)

Fig. 5.1 Manufactured antenna a) front view b) back view

5.1 Return loss measurement

Measurements of the antenna return loss were made using R&S®ZVL vector network analyzer after its calibration to 50 Ω. Since the antenna has a female (F) SMA connector, settings were made for a male (M) SMA connector. Start frequency was set to 2 GHz and stop frequency to 3 GHz to securely include the entire BLE band. Due to the influence of parasitic currents flowing through the connected analyzer's cable, three ferrite cores were attached to the antenna input to supress these currents.

Figure 5.2 shows a zoomed in view to the measurement outcome compared to simulated characteristics. Although having overall higher return loss values compared to the simulation model, the final manufactured product achieved the impedance matching condition within the whole considered operation band and can be declared as sufficiently working.

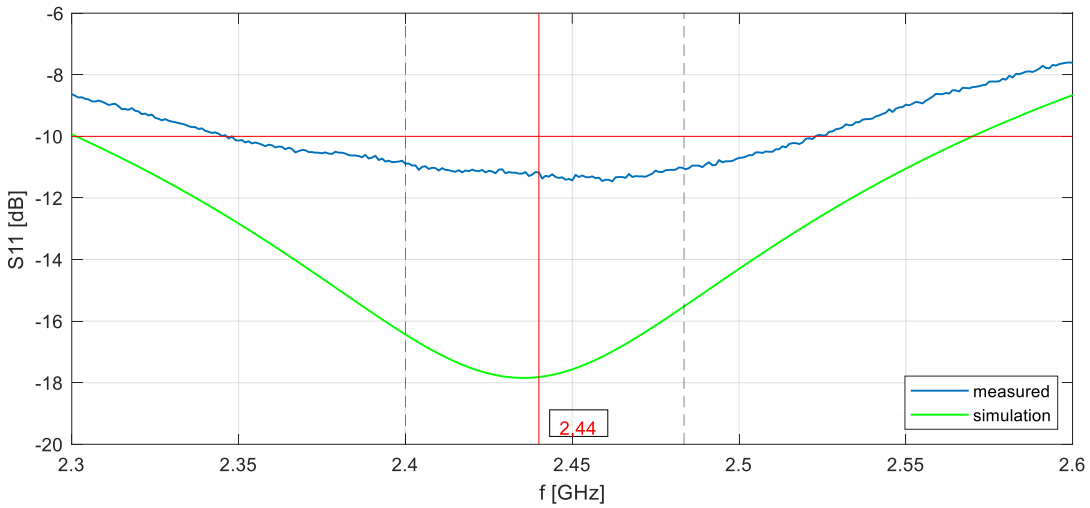

Fig. 5.2 Manufactured antenna return loss S_{11}

After examining the antenna in free space, a phantom wrapped in a foil was attached to its back side, simulating a situation of having a potential key in the car user's pocket. The foil is needed to keep the water present in phantom from vaporizing. To guarantee a fixed position of the antenna, an 8mm-thick polystyrene with relative permittivity close to 1 was placed between the antenna and the phantom. This setup was secured by a double-sided adhesive tape. For further measurements requirements, the layout was enhanced by adding another 15mm-thick layer of polystyrene behind the phantom to create a compact solid structure. Everything was supported by a few layers of adhesive tape. For visualisation, see the figure below.

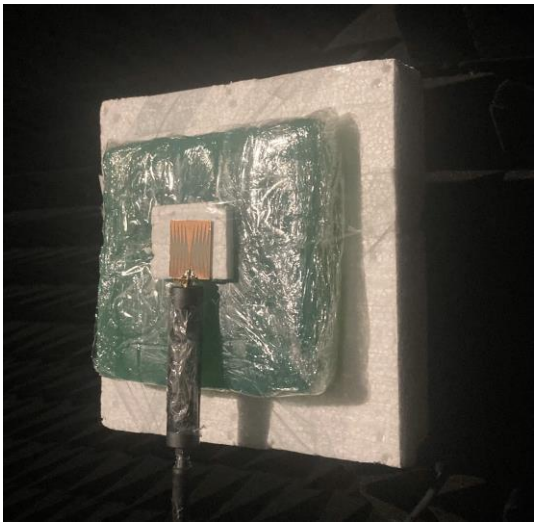

Fig. 5.3 Manufactured antenna with phantom setup

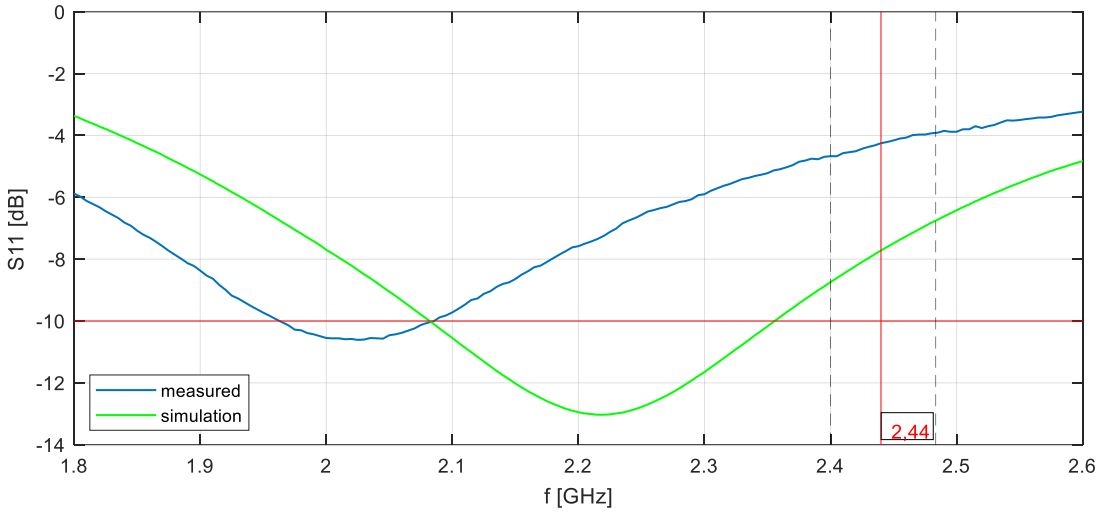

Fig. 5.4 Manufactured antenna with phantom return loss S_{11}

As expected, according to subchapter 4.3, adding a phantom to the antenna's near-field causes a shift to lower frequencies due to its high permittivity. It also shifts the return loss simulated values to higher values.

5.2 Radiation pattern measurement

A set of measurements were made in anechoic chamber both without and with the presence of phantom. The manufactured antenna was mounted to a mechanical arm that rotated around the chamber. After sending a signal with frequency 2.44 GHz to the electrically small magnetic dipole, a reference horn antenna connected to a vector network analyzer evaluated its radiation. The radiation patterns were examined in XY and YZ planes. Measurement for plane XZ was not made due to technical reasons.

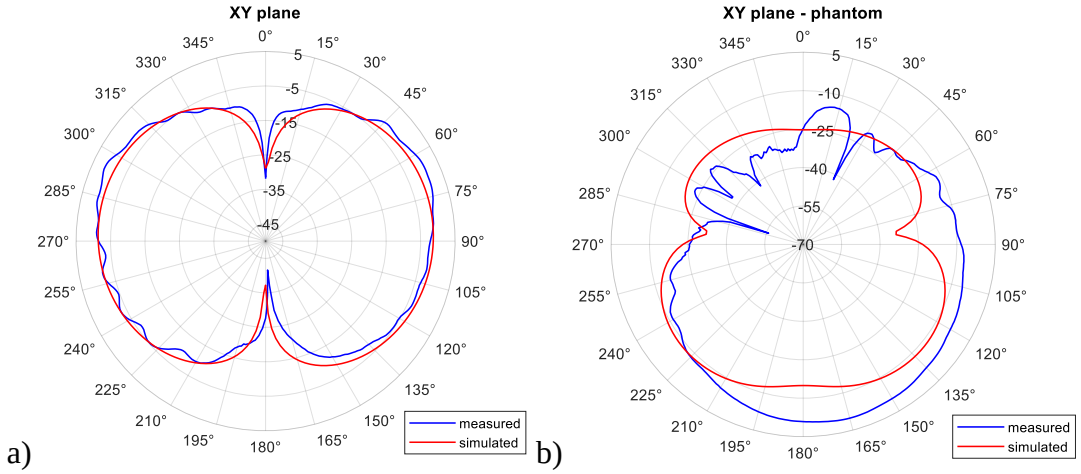

a) b)

Fig. 5.5 XY plane at 2.44 GHz a) without phantom b) with phantom

As shown in figure 5.5a), in free space, the antenna radiates as expected from the simulation. Subtle oscillation occurs due to unwanted signal reflection from the feeding

cable, room lighting or the rotating arm itself. Although most of the radiation is supressed with phantom presence, it can also be slightly amplified since the water present in the agar substance causes the phantom to act like a reflector (ground) which can be seen in direction of $\phi = 180°$ where the SMA connector was.

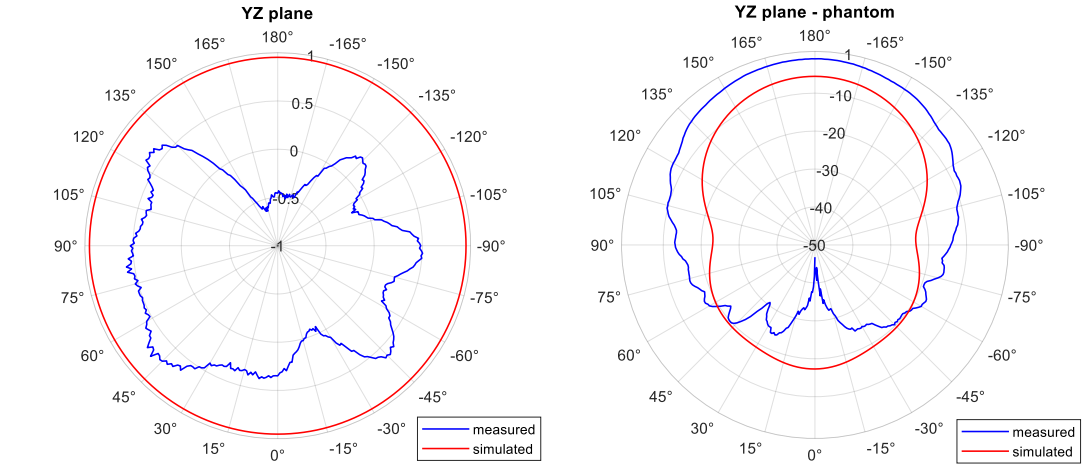

a) b)

Fig. 5.6 YZ plane at 2.44 GHz a) without phantom b) with phantom

Measurements in YZ plane, where the antenna should be omnidirectional, are presented in figure 5.6. The measured gain fluctuates with magnitude maximally around 1 dB and is overall smaller than simulated gain which can still be considered as omnidirectional radiation. Adding phantom behind the antenna caused a loss of radiation capability in the direction of phantom presence, i. e. when theta $\theta = 0°$. Again, slight gain amplification can be seen in 5.6b) due to phantom water presence.

5.3 Real environment measurement

To test the antenna usage with NXP KW45 for distance estimate, measurements in real environment were made. After connecting the antenna to the evaluation kit from NXP via SMA connectors, the electronic board was mounted onto a tripod. Distance change was done by moving the tripod around a circularly polarized reference antenna placed inside, in the middle of a car accordingly to marked positions on the ground, keeping the measured antenna turned directly to the reference antenna. The real measurement setup is shown in figure 5.7.

Marker-to-car distances were measured with a tape measure and noted. Their values and positions can be found in figure 5.8 created in [9]. Each marker has its number given accordingly to the position measurement sequence. Blue markers together form an inner circle and red markers are within an outer circle.

Distance evaluation in the BLE band using the manufactured antenna was performed both with and without a phantom. See figures 5.9 and 5.10 for results. Within the inner circle (markers 1-5), the antenna distance estimate without phantom was made with

absolute deviation not higher than 1 m. Positions 6 and 7 were evaluated with higher error rate due to presence of the right front car window metallic frame causing signal reflection. Generally, the antenna radiation was significantly affected by this frame, meaning that the evaluation errors occurrence was more frequent when estimating from the right side of the car. Finally, as expected, the phantom presence caused overall higher error rates since the antenna was not optimised for it.

a) 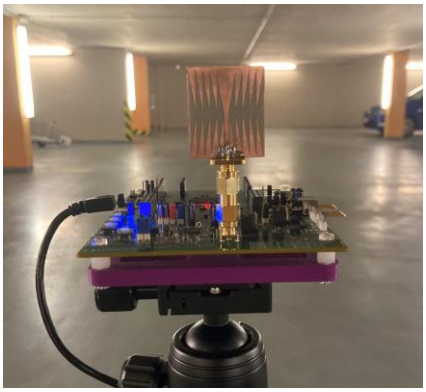 b) 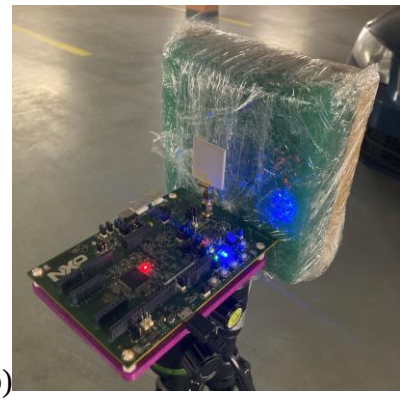

Fig. 5.7 Measurement setup a) with phantom b) without phantom

a) 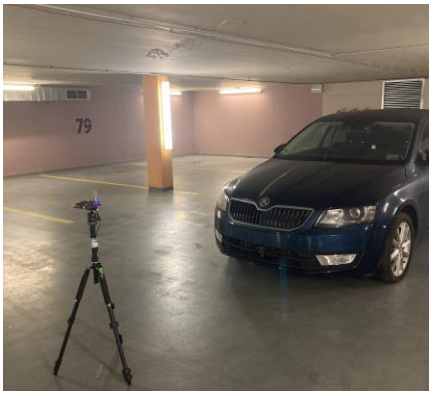

b) 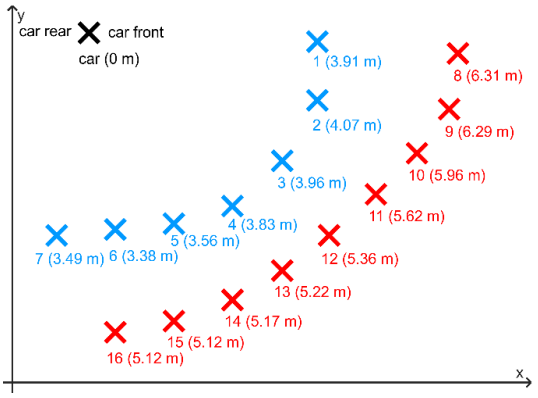

Fig. 5.8 Measurement setup a) towards the car b) in the term of markers

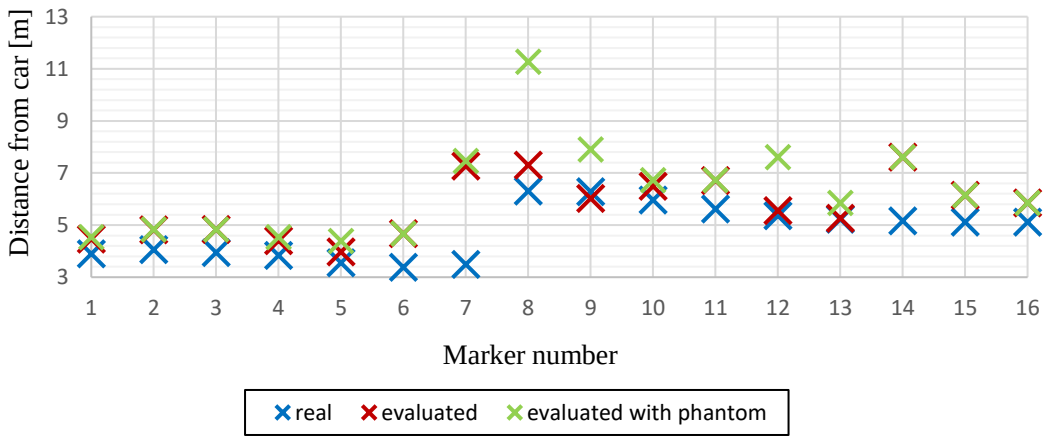

Fig. 5.9 Measurement results

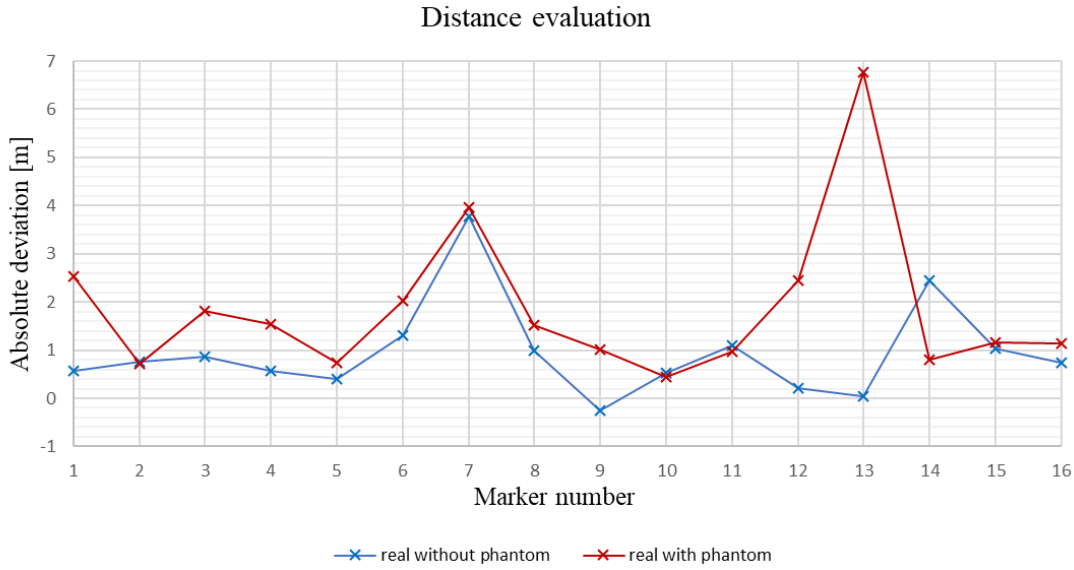

Fig. 5.10 Absolute deviation of distance evaluation outside the car

After finishing the measurements outside the car, the antenna was brought inside the car and measurements without phantom were made. Due to high signal reflection caused by the metallic parts of the car, the test proceeded with up to over 3 m deviation and thus was not repeated with phantom.

Table 5.1 Measurement inside the car

Position	real distance [m]	estimated distance [m]	absolute deviation [m]
front right	0.43	3.11	2.68
front left	0.40	2.56	2.16
rear left	0.96	1.97	1.01
rear centre	0.86	2.78	1.92
rear right	1.02	4.14	3.12

6. CONCLUSION

Overall, five different antennas manufacturable by PCB technology were designed within the thesis. Their characteristics were analysed and plotted in both, Ansys HFFS and MATLAB. Despite having the highest gain, both PIFA and L antenna did not achieve the desired radiation pattern. Wideband planar monopole had shown the needed impedance matching within the BLE band and had a suitable radiation pattern. However, it was dimensionally too large. Meander antenna design was not successful in any aspects. Thus, for the considered application, slot bow tie antenna was evaluated as the most suitable in the terms of bandwidth, radiation, gain and size.

The chosen antenna was optimized for usage with the microcontroller unit NXP KW45 by including an SMA connector into the design process. Adjustments were made within the antenna inner motif leaving the substrate dimensions unchanged. Further optimization was not made due to the base of the application.

Impact of the human presence in antenna's near-field was demonstrated by using a phantom in measurements. In general, organic tissue has high relative permittivity causing a decrease in antennas frequency bandwidth and thus, the antenna radiation can be supressed. This fact should be always considered when designing an antenna. However, phantoms vary in structure and fabrication complexity and therefore, the design process is not so straightforward.

Experimental measurements showed that the manufactured antenna characteristics are very close to the ones simulated in HFFS. Deviations are mainly caused by the real environment factors which were not considered in simulations. Additionally, the usage with NXP KW45 was demonstrated with the slot dipole being vertically oriented in real environment and the distance estimate was tested. The antenna radiation was significantly influenced by signal reflections from metallic parts of the car and the phantom presence leading to higher distance evaluation error rate.

LITERATURE

[1] ANALOG DEVICES. Remote Keyless Entry Systems Overview. Online. Analog Devices. Available from: https://www.analog.com/en/app-notes/remote-keyless-entry-systems-overview.html. [cit. 2024-01-02].

[2] ANSYS. Ansys HFSS Best-In-Class 3D High Frequency Structure Simulation Software. Online. 3D High Frequency Simulation Software. Available from: https://www.ansys.com/products/electronics/ansys-hfss. [cit. 2024-01-02].

[3] BALANIS, Constantine A. Antenna theory: analysis and design. Fourth edition. Hoboken: Wiley, [2016]. ISBN 978-1-118-64206-1.

[4] BLUETOOTH SPECIAL INTEREST GROUP [SIG]. Core Specification 5.4. Online. Bluetooth® Technology Website. Available from: https://www.bluetooth.com/specifications/core54-html/. [cit. 2024-01-02].

[5] BLUETOOTH SPECIAL INTEREST GROUP [SIG]. Blog Posts. Online. Bluetooth® Technology Website. Available from: https://www.bluetooth.com/blog/how-bluetooth-technology-uses-adaptive-frequency-hopping-to-overcome-packet-interference/. [cit. 2024-05-27].

[6] BLUETOOTH SPECIAL INTEREST GROUP [SIG]. Specifications and Documents. Online. Bluetooth® Technology Website. Available from: https://www.bluetooth.com/specifications/specs/channel-sounding-cr-pr/. [cit. 2024-01-02].

[7] Cinch Connectivity Solutions, Inc. 142-0861-851 Assembly Instruction. Online. Available from: https://www.cinch.com/media/assembly-instructions/products/rf-microwave/connectors/ai-ccs-john-sma-high-frequency-end-launch-connectors-application-note.pdf. [cit. 2024-05-27].

[8] COMMENS, Math. From Chips to Ships, Solve Them All With HFSS. Online. Ansys. Available from: https://www.ansys.com/blog/from-chips-to-ships-hfss. [cit. 2024-01-02].

[9] GeoGebra®. GeoGebra Classic. Online. Available from: https://www.geogebra.org/classic. [cit. 2024-05-27].

[10] KAMEI, T.; UTSUMI, Y.; QUOC DINH, N. a THANH, N. Wide-Band Coaxial-to-Coplanar Transition. Online. IEICE Transactions on Electronics. 2007, vol. E90-C, c. 10, pp. 2030-2036. ISSN 0916-8524. Available from: https://doi.org/10.1093/ietele/e90-c.10.2030. [cit. 2024-05-27].

[11] MCMAHILL, Dan. Coplanar Waveguide Analysis/Synthesis Calculator. Online. Dan McMahill. Available from: https://wcalc.sourceforge.net/cgi-bin/coplanar.cgi [cit. 2024-01-02].

[12] MIKULČÁK, Jiří. Matematické, fyzikální a chemické tabulky pro střední školy. 3. vyd. Pomocné knihy pro žáky (Prometheus). Praha: Prometheus, 1995. ISBN 80-85849-84-4.

[13] NXP Semiconductors. KW45B41Z Evaluation Kit Board. Product Details. Online. Available from:.https://www.nxp.com/design/design-

center/software/development-software/mcuxpresso-software-and-tools-/kw45b41z-evaluation-kit-with-bluetooth-low-energy:KW45B41Z-EVK. [cit. 2024-05-27].

[14] NXP Semiconductors. KW45B41Z Evaluation Kit Board. Online. In: https://www.nxp.com/design/design-center/software/development-software/mcuxpresso-software-and-tools-/kw45b41z-evaluation-kit-with-bluetooth-low-energy:KW45B41Z-EVK. Available from: https://www.nxp.com/assets/images/en/dev-board-image/KW45B41Z-EVK-IMG.jpg. [cit. 2024-05-27].

[15] NXP Semiconductors. User Guide: Antennas for Channel Sounding Applications. NXP B. V., 2024, 39 p. UG10107. Available from: https://www.nxp.com/. Password requested. [cit. 2024-05-27].

[16] PELKA, Mathias; BOLLMEYER, Christian a HELLBRUCK, Horst. Accurate radio distance estimation by phase measurements with multiple frequencies. Online. In: 2014 International Conference on Indoor Positioning and Indoor Navigation (IPIN). IEEE, 2014, s. 142-151. ISBN 978-1-4673-8054-6. Available from: https://doi.org/10.1109/IPIN.2014.7275478. [cit. 2024-01-02].

[17] PITRA, Kamil and RAIDA, Zbynek. Small antenna for aerobatic aircraft. Online. In: 2012 6th European Conference on Antennas and Propagation (EUCAP). IEEE, 2012, s. 143-146. ISBN 978-1-4577-0920-3. Available from: https://doi.org/10.1109/EuCAP.2012.6205952. [cit. 2024-05-26].

[18] PROSPECTOR, Ul. Arlon® 25N. Online. Prospector. Available from: https://materials.ulprospector.com/en/document?e=120881. [cit. 2024-01-02].

[19] RAIDA, Zbyněk; ČERNOHORSKÝ, Dušan; GALA, Dalimil; GOŇA, Stanislav; NOVÁČEK, Zdeněk. et al. Kapitola 4: Antény. Online. Publisher not found. Available from: https://www.radio.feec.vutbr.cz/raida/multimedia/index.php?nav=4. [cit. 2024-01-02].

[20] RAIDA, Zbyněk; LÁČÍK, Jaroslav; MRNKA, Michal; PUSKELY, Jan; MIKULÁŠEK, Tomáš et al. Elektromagnetické struktury v blízkosti živých tkání. V Brně: Vysoké učení technické, 2016. ISBN 978-80-214-5449-1.

[21] SPHERO TEAM. Bluetooth Low Energy Tech vs. Bluetooth. Online. Sphero. Available from: https://sphero.com/blogs/news/bluetooth-low-energy-vs-bluetooth. [cit. 2024-01-02].

[22] VAIS Technology. Remote Keyless Entry vs Keyless Entry: What's the Difference?. Online. 2024. Available from: https://vaistech.com/remote-keyless-entry-vs-keyless-entry-whats-the-difference/. [cit. 2024-05-27].

SYMBOLS AND ABBREVIATIONS

Abbreviations:

3D	three-dimensional
AFH	Adaptive Frequency Hopping
BLE	Bluetooth Low Energy
CAN	Control Area Network
CPW	Coplanar Waveguide
CS	Channel Sounding
DC	direct current
E-plane	plane containing the electric field vector
F	female
FDMA	Frequency Division Multiple Access
FEM	Finite Element Method
FHSS	Frequency Hopping Spread Spectrum
GCPW	Grounded Coplanar Waveguide
GND	ground
HFSS	High Frequency Structure Simulator
H-plane	plane containing the magnetic field vector
ISM	industrial, scientific and medical
LIN	Local Interconnect Network
M	male
MCU	microcontroller unit
MoM	Method of Moments
PBR	phase-based ranging
PCB	Printed Circuit Board
PEPS	Passive Entry Passive Start
PIFA	Planar Inverted F Antenna
RF	radiofrequency
RKE	Remote Keyless Entry
RTT	round-trip time
SMA	SubMiniature version A
TDMA	Time Division Multiple Access
ToA	Time of Arrival
ToD	Time of Departure
ToF	Time of Flight

Symbols:

c	speed of light in vacuum	(m/s)
f	frequency	(Hz)
f_c	centre frequency	(Hz)
f_{c_min}	maximal centre frequency	(Hz)
f_{c_max}	minimal centre frequency	(Hz)
ToA_i	time of data arrival towards the initiator	(s)
ToD_i	time of data departure from the initiator	(s)
ToA_r	time of data arrival towards the reflector	(m)
ToD_r	time of data departure from the initiator	(m)
λ	wavelength	(m)
x	distance between two devices	(m)
$\Delta\varphi$	phase shift	(°)
ε_r	relative permittivity	(-)
L	length	(m)
n	number of iterations	(-)
k	index	(-)
s	gap between CPW conductors	(m)
w_f	CPW signal conductor width	(m)